SIAM/ASA J. Uncertainty Quantification
Vol. 13, No. 2, pp. 639–678

© 2025 Society for Industrial and Applied Mathematics
and American Statistical Association

A Convergent Interacting Particle Method for Computing KPP Front Speeds in Random Flows*

Tan Zhang†, Zhongjian Wang‡, Jack Xin§, and Zhiwen Zhang¶

Abstract. This paper aims to efficiently compute the spreading speeds of reaction-diffusion-advection fronts in divergence-free random flows under the Kolmogorov–Petrovsky–Piskunov (KPP) nonlinearity. We develop a stochastic interacting particle method (IPM) for the reduced principal eigenvalue (Lyapunov exponent) problem of an associated linear advection-diffusion operator with spatially random coefficients. The Fourier representation of the random advection field and the Feynman–Kac formula of the principal eigenvalue (Lyapunov exponent) form the foundation of our method, which is implemented as a genetic evolution algorithm. The particles undergo advection-diffusion and mutation/selection through a fitness function that originates in the Feynman–Kac semigroup. We analyze the convergence of the algorithm based on operator splitting and present numerical results on representative flows, such as 2D cellular flow and 3D Arnold–Beltrami–Childress (ABC) flow under random perturbations. The 2D examples serve as a consistency check with semi-Lagrangian computation. The 3D results demonstrate that IPM, being mesh-free and self-adaptive, is easy to implement and efficient for computing front spreading speeds in the advection-dominated regime for high-dimensional random flows on unbounded domains where no truncation is needed.

Key words. KPP front speeds, random flows, Feynman–Kac semigroups, interacting particle method, convergence analysis

MSC codes. 35K57, 47D08, 65C35, 65L20, 65N25

DOI. 10.1137/23M1604564

1. Introduction.

Front propagation in complex fluid flows is a nonlinear phenomenon commonly found in many scientific and technological areas, such as chemical reaction fronts in liquid, transport in porous media, and turbulence combustion [37]. If the fluid velocity field is simulated by stochastic processes with known statistics, one challenging mathematical problem

*Received by the editors January 2, 2024; accepted for publication (in revised form) January 6, 2025; published electronically April 28, 2025.
https://doi.org/10.1137/23M1604564
Funding: The work of the second author was partially supported by NTU-SUG and MOE AcRF (RG17/24). The work of the third author was partially supported by NSF grants DMS-2219904, DMS-2151235, and DMS-2309520. The work of the fourth author was partially supported by the National Natural Science Foundation of China (Projects 92470103 and 12171406), the Hong Kong RGC grant (Projects G-HKU702/18, 17307921, and 17304324), the Outstanding Young Researcher award of HKU (2020-21), Seed Funding for Basic Research, and Seed Funding for Strategic Interdisciplinary Research Scheme 2021/22 (HKU).

†Department of Mathematics, The University of Hong Kong, Pokfulam Road, Hong Kong SAR, People's Republic of China (thta@connect.hku.hk).
‡Division of Mathematical Sciences, School of Physical and Mathematical Sciences, Nanyang Technological University, Singapore 637371 (zhongjian.wang@ntu.edu.sg).
§Department of Mathematics, University of California at Irvine, Irvine, CA 92697 USA (jxin@math.uci.edu).
¶Corresponding author. Department of Mathematics, The University of Hong Kong, Pokfulam Road, Hong Kong SAR, People's Republic of China, and Materials Innovation Institute for Life Sciences and Energy (MILES), HKU-SIRI, Shenzhen, People's Republic of China (zhangzw@hku.hk).

Downloaded 05/24/25 to 128.195.71.97 . Redistribution subject to SIAM license or copyright; see https://epubs.siam.org/terms-privacy

Copyright © by SIAM and ASA. Unauthorized reproduction of this article is prohibited.

Downloaded 05/24/25 to 128.195.71.97 . Redistribution subject to SIAM license or copyright; see https://epubs.siam.org/terms-privacy

is to characterize and compute the propagation velocity of the front (the dynamic asymptotic stability of the front in the large time limit) by utilizing the governing partial differential equations (PDEs). An extensively studied model is the following reaction-diffusion-advection (RDA) equation with Kolmogorov–Petrovsky–Piskunov (KPP) nonlinearity [12]:

$$u_t = \kappa \Delta_{\boldsymbol{x}} u + (\boldsymbol{v} \cdot \nabla_{\boldsymbol{x}}) u + f(u), \quad t \in \mathbb{R}^+, \quad \boldsymbol{x} = (x_1, \ldots, x_d)^T \in \mathbb{R}^d. \tag{1.1}$$

Here in equation (1.1), u is the concentration of reactant or population, κ is the diffusion constant, and $\boldsymbol{v}$ is a prescribed incompressible velocity field. We focus on the case with KPP reaction term $f(u) = u(1-u)$ satisfying $f(u) \le u f'(0)$. In the following analysis and numerical examples, we will fix $\kappa = 1$ while changing the magnitude of the velocity field $\boldsymbol{v}$ or, equivalently, varying Péclet number Pe, which measures the relative strength of advection and diffusion.

The propagation of reaction-diffusion fronts in fluid flows has been an actively researched field for decades [6, 35, 17, 36, 1, 24, 25, 37, 22]. The dynamic asymptotic stability of the system (1.1) means that if the initial data are prescribed in the form $u_0(\boldsymbol{x}) = U_c(\boldsymbol{x}) + \tilde{u}(\boldsymbol{x})$, where $U_c(\boldsymbol{x})$ is a front profile corresponding to the wave speed c with propagation direction $\boldsymbol{z}$, and $\tilde{u}(\boldsymbol{x})$ is a smooth and spatially decaying perturbation, then $u(\boldsymbol{x}, t)$ converges to $U_c(\boldsymbol{x} - ct\boldsymbol{z} + \boldsymbol{\xi}_0)$ in a suitably weighted Banach space as $t \to \infty$ for some constant vector $\boldsymbol{\xi}_0$. Due to the spatial translation-invariance of the original equation, it may have a family of traveling fronts for each allowable wave speed c. We shall refer to the front moves with the slowest speed in absolute value as the critical front and to its corresponding wave speed $c = c^*$ as the front speed [23, 36]. The linear corrector equation and the variational formula aided the computation of KPP front speeds. For spatially periodic velocity field $\boldsymbol{v} = \boldsymbol{v}(\boldsymbol{x})$, the minimal front speed formula was known [5, 6] around the 1980s as $c^*(\boldsymbol{z}) = \inf_{(\boldsymbol{z}, \lambda \boldsymbol{e}) > 0} \mu(\lambda \boldsymbol{e}) / (\boldsymbol{z}, \lambda \boldsymbol{e})$. Here $\boldsymbol{z} \in \mathbb{R}^d$ is the front propagation direction, and $\mu(\lambda \boldsymbol{e})$ is the principal eigenvalue of the linear advection-reaction-diffusion operator $\mathcal{A}^\lambda$ parameterized by dual unit vector $\boldsymbol{e} \in \mathbb{R}^d$ and $\lambda \in \mathbb{R}$,

$$\mathcal{A}^\lambda \equiv \kappa \Delta_{\boldsymbol{x}} \cdot + (-2\kappa\lambda \boldsymbol{e} + \boldsymbol{v}) \cdot \nabla_{\boldsymbol{x}} \cdot + (\kappa \lambda^2 - \lambda \boldsymbol{v} \cdot \boldsymbol{e} + f'(0)), \tag{1.2}$$

on a d-dimensional torus $\mathbb{T}^d$. When $\boldsymbol{v}$ is space-time ergodic, the c^* variational formula can be generalized to the cases [25] with μ being the principal Lyapunov exponent and $\mathbb{R}^d$ in place of $\mathbb{T}^d$. Existing works include the adaptive finite element method (FEM) for steady flows [31, 30]; edge-averaged FEM with algebraic multigrid acceleration [41] for two-dimensional (2D) time-periodic flows; and the semi-Lagrangian (SL) method for 2D random flows [24]. When flow is random with large amplitude and spatially 3D, the FEM and SL calculations of μ become incredibly expensive. An alternative is the (fully Lagrangian, mesh-free, and self-adaptive) interacting particle method (IPM) [15], which has been successfully studied for cellular and chaotic flows. This motivates us to develop IPM for computing KPP front speeds in random flows in this paper.

We first combine operator splitting and random Fourier methods to approximate the underlying linear advection-diffusion operator (equation (2.8)) and then leverage the Feynman–Kac (FK) representation of the parabolic evolution and develop an IPM to compute c^*. Since directly approximating the FK formula is unstable, we study a normalized version for μ based on the corresponding FK semigroups. Using perturbation theory (Proposition 3.1), we guarantee the existence of μ when a relatively small random field with an equispaced discrete

Copyright © by SIAM and ASA. Unauthorized reproduction of this article is prohibited.

Downloaded 05/24/25 to 128.195.71.97 . Redistribution subject to SIAM license or copyright; see https://epubs.siam.org/terms-privacy

spectrum is added to a deterministic flow on $\mathcal{D}$, where $\mathcal{D} = [0, \frac{1}{\Delta k}]^d$ is a d-dimensional torus and Δk is the frequency step of $\boldsymbol{v}$. The random flow $\boldsymbol{v}$ with the equispaced discrete spectrum is realizable by the random Fourier method and approximated by the series $\{\boldsymbol{v}_j\}$ along with the convergence of their expectations in $L^2(\mathcal{D})$ (i.e., as $j \to \infty, \mathbb{E}[||\boldsymbol{v} - \boldsymbol{v}_j||_{L^2(\mathcal{D})}] \to 0$; equation (3.38)) and μ approximations (Theorem 3.7). Next, we estimate the approximation generated by the random Fourier method associated with the solution operator of nonautonomous evolution equations (Theorem 3.8). It demonstrates that the solution operator approximated by the random Fourier method has a convergence rate of $O(\sqrt{(\Delta t)^2 + ||\boldsymbol{v} - \boldsymbol{v}_j||^2_{L^2(\mathcal{D})}})$, where Δt denotes the discrete time step. We also provide an error estimate of the IPM on c^* in random flows on $\mathcal{D}$. It indicates that *the IPM has the following convergence result:*

$$\mu_{IPM}(\lambda) = \mu(\lambda) + O\left(\left(1 - \frac{\theta}{\vartheta}\right)^M\right) + O((\Delta t)^{\frac{1}{2}}) + O(||\boldsymbol{v} - \tilde{\boldsymbol{v}}||_{L^2(\mathcal{D})}), \tag{1.3}$$

where μ, μ_{IPM} are the corresponding principal eigenvalues of the original system and the IPM. $\tilde{\boldsymbol{v}}$ is an approximation to $\boldsymbol{v}$ and generated by the random Fourier method. $0 < \theta < \vartheta$ are parameters, and M is the iteration number (Theorem 3.9).

Numerically, we observe the convergence of c^* in the large volume limit of $\mathcal{D}$ to the values from a direct IPM computation on $\mathbb{R}^d$, encouraging a future study along the line of periodization of stochastic homogenization (see [11, 7, 13] for elliptic problems). Flexible for both $\mathcal{D}$ and $\mathbb{R}^d$, IPM is advantageous for high-dimensional and stochastic flows where the issue of unbounded domain arises in the simulation of (1.2) and is expensive for traditional Eulerian methods. For time complexity, let N_x denote the number of grid points in each dimension of Eulerian methods and N represent the Monte Carlo number in IPM. With the same iteration number n and time step Δt, the time complexity of traditional Eulerian methods (e.g., semi-Lagrangian + Crank–Nicolson method in [24]) is $O((N_x)^d)$, while the IPM has a time complexity of $O(Nd)$. Comparing the two approaches, we see that IPM is *self-adaptive and free from domain truncation.* For particle methods on related effective diffusivity problems in periodic and stochastic flows, see [27, 28, 29, 32, 33, 14, 34, 40].

The rest of the paper is organized as follows. In section 2, we review the background of the random Fourier method and present an IPM for computing c^* in random flows. In section 3, we provide the error estimate of the approximation to the solution operator and convergence rate. In section 4, we validate IPM with a semi-Lagrangian method on 2D examples and carry out numerical experiments to show its accuracy in spatially periodic flows in agreement with known theoretical results. Meanwhile, experiments on the time complexity of the semi-Lagrangian method in a 3D periodic flow have been conducted. Then we investigate the influence of random perturbations on c^* and show the distribution of particles with different magnitudes of perturbation. Most notable is the randomly perturbed ABC flows, whose vortical structures are increasingly smeared as the random perturbations are strengthened, and c^* is reduced accordingly. We discuss a shift normalization of IPM on $\mathbb{R}^d$ to realize its convergence to an invariant measure. Concluding remarks are given in section 5, with most of the proofs left to the appendices.

2. Efficient IPM for KPP front speeds.

We develop the Lagrangian IPM for computing c^* in random flows.

Copyright © by SIAM and ASA. Unauthorized reproduction of this article is prohibited.

Downloaded 05/24/25 to 128.195.71.97 . Redistribution subject to SIAM license or copyright; see https://epubs.siam.org/terms-privacy

2.1. Random fields realization. Several earlier works on calculating the KPP front speeds of random fields required a certain compactness of the domain or regularity of the random fields. In [24], an infinite channel with a finite size cross section and a random shear flow imposed on the cross section is considered. In [25], the author assumes the random velocity field is uniformly bounded in the spatial domain $\mathbb{R}^d$. Considering the compactness of the functional space, we would like to consider a kind of random velocity field with an equispaced discrete spectrum in this paper. For a random velocity field, $v(x,\omega)$, with the equispaced discrete spectrum, it can be represented as a sum of uncorrelated harmonic oscillations, i.e.,

$$v(x,\omega) = \sum_{j=-\infty}^{\infty} e^{-2\pi i j\Delta k x} E^{1/2}(|j|\Delta k)\Delta\tilde{W}_j, \tag{2.1}$$

where $E(k)$ is a given spectral density, ω is an element of the probability space describing all possible environments, and the complex random variables $\Delta\tilde{W}_j$ are defined in terms of the complex white noise process,

$$\Delta\tilde{W}_j = \int_{j-\Delta k/2}^{j+\Delta k/2} d\tilde{W}(k), \tag{2.2}$$

where $d\tilde{W}(k)$ represents a complex Gaussian white noise. Of course, stationary random processes with a discrete spectrum are far from the only kind of stationary processes. However, it turns out that any stationary process can be obtained as the limit of a sequence of processes with discrete spectra [39].

To approximate the random velocity field $v(x,\omega)$, we use random Fourier methods [16] for producing a random velocity field $\tilde{v}(x,\omega)$. For ease of implementation, we require $\tilde{v}(x,\omega)$ to be described by combinations of a finite number of random variables. The random Fourier method can be verified by computing the average of mean-square displacement among N_r independent realizations $\{\tilde{v}^j\}_{j=1}^{N_r}$ of the approximate velocity fields which are generated by successive calls to the random number generator (different random seeds). By Riemann sum approximation over a finite partition of $2N_F+1$ equal-width intervals of width Δk, we define $k_{max} = (N_F + \frac{1}{2})\Delta k$. This partition extends over a finite interval $[-k_{max}, k_{max}]$. We can get the following Riemann–Stieltjes sum for the approximating velocity field:

$$\tilde{v}(x,\omega) = \sum_{j=-N_F}^{N_F} e^{-2\pi i j\Delta k x} E^{1/2}(|j|\Delta k)\Delta\tilde{W}_j, \tag{2.3}$$

where $\{\Delta\tilde{W}_j\}_{j=1}^{N_F}$ are statistically independent complex Gaussian variables, and $\Delta\tilde{W}_0$ is a real Gaussian variable with mean zero and variance Δk independent from all other variables. Therefore we can transform (2.3) into

$$\tilde{v}(x,\omega) = E^{1/2}(0)\Delta\tilde{W}_0 + 2\mathbf{Re}\sum_{j=1}^{N_F} e^{-2\pi i j\Delta k x} E^{1/2}(|j|\Delta k)\Delta\tilde{W}_j, \tag{2.4}$$

which shares the same distribution. Here **Re** denotes the real part of the following expression. By expanding the complex random variable $\Delta\tilde{W}_j$ into real and imaginary parts, we obtain a concise expression of the approximate velocity field as a discrete sum of real Fourier modes. The approximate velocity field is

Copyright © by SIAM and ASA. Unauthorized reproduction of this article is prohibited.

$$\tilde{v}(x,\omega)=\sum_{j=0}^{N_F}\sqrt{2E(k_j)\Delta k_j}[\zeta_j\cos(2\pi k_j x)+\eta_j\sin(2\pi k_j x)], \tag{2.5}$$

where $k_j = j\Delta k$ denote the locations of equally spaced grid points, and $\Delta k_j = \Delta k$ for $j = 1,2,\ldots,N_F$ and $\Delta k_0 = \frac{1}{2}\Delta k$. The $\{\zeta_j\}_{j=0}^{N_F}$ and $\{\eta_j\}_{j=0}^{N_F}$ are independent Gaussian variables with mean zero and variance one.

The exact correlation function of random field $v(x,\omega)$ with given $E(k)$ is

$$R(x)=\langle v(x_0,\omega)v(x_0+x,\omega)\rangle=2\sum_{j=0}^{\infty}E(k_j)\Delta k_j\cos(2\pi k_j x). \tag{2.6}$$

As $\Delta k\to 0$, (2.6) will be an approximation to the integral $\int_0^\infty \cos(2\pi kx)E(k)dk$. Meanwhile, the correlation function of the Fourier generated random field $\tilde{v}(x,\omega)$ is

$$\begin{aligned}\tilde{R}(x)=&\sum_{j=0}^{N_F}\left(\sqrt{2E(k_j)\Delta k_j}\right)^2[\cos(2\pi k_j x_0)\cos(2\pi k_j(x+x_0))\\ &+\sin(2\pi k_j x_0)\sin(2\pi k_j(x+x_0))]=\sum_{j=0}^{N_F}2E(k_j)\Delta k_j\cos(2\pi k_j x).\end{aligned} \tag{2.7}$$

By comparing the two correlation functions (2.6) and (2.7), we find that $\tilde{R}(x)$ is just the finite truncation of $R(x)$. As the number of Fourier modes N_F gets larger, this approximation will become more accurate. In our numerical experiments, we select these two parameters according to the correlation length of energy spectral density.

2.2. Computing μ by FK semigroup. Let us consider $\boldsymbol{v}=\boldsymbol{v}(\boldsymbol{x},\omega)$, a mean zero and divergence-free flow field, to be constructed by a sum of a deterministic space term with period 1 and a stochastic term. The stochastic term is a mean zero, stationary, and ergodic random field defined by (2.1). We assume that the realizations of $\boldsymbol{v}(\boldsymbol{x},\omega)$ are almost surely divergence-free. To compute the KPP front speed $c^*(\boldsymbol{z})$ along direction $\boldsymbol{z}$, we denote q as the solution to the linearized corrector equation with $(\boldsymbol{z},\boldsymbol{e})>0$ as follows:

$$q_t=\mathcal{A}q\overset{\text{def}}{=}\kappa\Delta_{\boldsymbol{x}}q+(-2\kappa\lambda\boldsymbol{e}+\boldsymbol{v})\cdot\nabla_{\boldsymbol{x}}q+(\kappa\lambda^2-\lambda\boldsymbol{v}\cdot\boldsymbol{e}+f'(0))q, \tag{2.8}$$

with compactly supported nonnegative initial condition $q(\boldsymbol{x},0)\not\equiv 0$. Recall that the minimal front speed in $\boldsymbol{z}$ is $c^*(\boldsymbol{z})=\inf_{(\boldsymbol{z},\lambda\boldsymbol{e})>0}\mu(\lambda\boldsymbol{e})/(\boldsymbol{z},\lambda\boldsymbol{e})$, where

$$\mu(\lambda\boldsymbol{e})=\lim_{t\to+\infty}\frac{1}{t}\ln\int_{\mathbb{R}^d}q(\boldsymbol{x},t)d\boldsymbol{x}, \tag{2.9}$$

also known as the principal Lyapunov exponent of (2.8). We define $c(\boldsymbol{x},\omega)=(\kappa\lambda^2-\lambda\boldsymbol{v}(\boldsymbol{x},\omega)\cdot\boldsymbol{e}+f'(0))$. To design the IPM, we split the operator $\mathcal{A}$ into $\mathcal{A}=\mathcal{L}+\mathcal{C}$, where $\mathcal{L}$ and $\mathcal{C}$ are defined by

$$\mathcal{L}q\overset{\text{def}}{=}\kappa\Delta_{\boldsymbol{x}}q+(-2\kappa\lambda\boldsymbol{e}+\boldsymbol{v})\cdot\nabla_{\boldsymbol{x}}q, \tag{2.10}$$

Downloaded 05/24/25 to 128.195.71.97 . Redistribution subject to SIAM license or copyright; see https://epubs.siam.org/terms-privacy

Copyright © by SIAM and ASA. Unauthorized reproduction of this article is prohibited.

$$\mathcal{C}q \overset{\text{def}}{=} (\kappa\lambda^2 - \lambda \boldsymbol{v}\cdot\boldsymbol{e} + f'(0))q. \tag{2.11}$$

Then for each random realization, to approximate the operator $\mathcal{L}$, we define the following SDE system:

$$dX_s^{t_2,t_1,\boldsymbol{x}} = \boldsymbol{b}(X_s^{t_2,t_1,\boldsymbol{x}})\,ds + \sqrt{2\kappa}\,d\mathbf{w}(s), \quad X_{t_1}^{t_2,t_1,\boldsymbol{x}} = \boldsymbol{x}, \quad t_2 \geq s \geq t_1, \tag{2.12}$$

where $\boldsymbol{b} = -2\kappa\lambda\boldsymbol{e} + \boldsymbol{v}$ is the drift term, and $\mathbf{w}(s)$ is a d-dimensional Brownian motion independent of ω. The FK formula is

$$\mu(\lambda\boldsymbol{e}) = \lim_{t\to+\infty} \frac{1}{t} \ln \mathbb{E}\left(\exp\left(\int_0^t c(X_s^{t,0,\boldsymbol{x}})ds\right)\right). \tag{2.13}$$

Here the expectation is over the probability space induced by the d-dimensional Brownian motion $\mathbf{w}(t)$. For a given $\boldsymbol{e}$ and its corresponding operator $\mathcal{A}$ in the following analysis, we denote $\mu(\lambda) = \mu(\lambda\boldsymbol{e})$ for simplicity. Only during the computation of front speed c^* do we search $\boldsymbol{e}$ to minimize $\mu(\lambda\boldsymbol{e})/(\boldsymbol{z},\lambda\boldsymbol{e})$ subject to $(\boldsymbol{z},\boldsymbol{e}) > 0$.

Comparing the computation in formulas (2.9) and (2.13), we see that the FK formula provides an alternative strategy for designing (Lagrangian) particle methods to compute $\mu(\lambda)$ and overcome the drawbacks in the traditional Eulerian methods, especially in the cases when the magnitude of $\boldsymbol{v}$ is large or the dimensional d is high (e.g., $d = 3$). Directly applying the FK formula (2.13) is unstable as the sample paths visiting the maximal points of the potential c make up the main contribution to the expectation $\mathbb{E}$ in (2.13). This may lead to inaccurate or even divergent results. A more accurate strategy for the computation of $\mu(\lambda)$ is to study the convergence of the FK group associated with the above stochastic differential equations (SDEs) (2.12) and the potential c. From (2.1), $\boldsymbol{v}(\boldsymbol{x},\omega)$ will have a period $1/\Delta k$ in each spatial dimension if we set $1/\Delta k \in \mathbb{N}^+$. Specifically, let $\mathcal{D} = [0, \frac{1}{\Delta k}]^d$ denote the d-dimensional torus with the periodic boundary condition, $\mathcal{P}(\mathcal{D})$ denoting the set of probability measures over $\mathcal{D}$ and $S = \mathcal{C}^\infty(\mathcal{D})$. Unless otherwise specified, the norms taken in the rest of this paper are all on the domain $\mathcal{D}$. Then let $Q_{\cdot,\cdot}$ denote the evolution operator which is associated with the process $X_s^{t_2,t_1,\boldsymbol{x}}$ in the SDE system; i.e., for any measure $m \in P(\mathcal{D})$ and any function $\phi \in S$, we have

$$m(Q_{t_2,t_1}\phi) = \mathbb{E}_{\boldsymbol{x}\sim m}\left(\phi(X_{t_2}^{t_2,t_1,\boldsymbol{x}})\right). \tag{2.14}$$

Similarly, we define the associated weighted counterpart as

$$m(Q^c_{t_2,t_1}\phi) = \mathbb{E}_{\boldsymbol{x}\sim m}\left(\phi(X_{t_2}^{t_2,t_1,\boldsymbol{x}})\exp\left(\int_{t_1}^{t_2} c(X_s^{t_2,t_1,\boldsymbol{x}})ds\right)\right). \tag{2.15}$$

The $\mathcal{L}(t_1)$ and $\mathcal{A}(t_1)$ are the infinitesimal generators of two evolution operators Q_{t_2,t_1} and $Q^c_{t_2,t_1}$. By the definition of $Q^c_{t_2,t_1}$ and as in [4, 2], we define the FK operator $\Phi^c_{t_2,t_1}$ by

$$\Phi^c_{t_2,t_1}(m)(\phi) = \frac{m(Q^c_{t_2,t_1}\phi)}{m(Q^c_{t_2,t_1}1)} = \frac{\mathbb{E}_{\boldsymbol{x}\sim m}(\phi(X_{t_2}^{t_2,t_1,\boldsymbol{x}})\exp(\int_{t_1}^{t_2} c(X_s^{t_2,t_1,\boldsymbol{x}})ds))}{\mathbb{E}_{\boldsymbol{x}\sim m}(\exp(\int_{t_1}^{t_2} c(X_s^{t_2,t_1,\boldsymbol{x}})ds))}. \tag{2.16}$$

Due to steady velocity fields here, we denote $Q^c_{t,0} = Q^c_t$ and $\Phi^c_{t,0} = \Phi^c_t$. Let m_c denote the invariant measure of Φ^c_t which satisfies $\Phi^c_t(m_c) = m_c$. It is straightforward to verify the following property of the FK semigroup Φ^c_t [15].

Copyright © by SIAM and ASA. Unauthorized reproduction of this article is prohibited.

Downloaded 05/24/25 to 128.195.71.97 . Redistribution subject to SIAM license or copyright; see https://epubs.siam.org/terms-privacy

Downloaded 05/24/25 to 128.195.71.97 . Redistribution subject to SIAM license or copyright; see https://epubs.siam.org/terms-privacy

Proposition 2.1. *For any $m \in \mathcal{P}(\mathcal{D})$ and $\phi \in S$, there exists $C_{\mathcal{A}} > 0$ such that*

$$\left|\Phi_t^c(m)(\phi) - \int_{\mathcal{D}} \phi dm_c\right| \leq C_{\mathcal{A}}||\phi|| \exp(-\delta_c t), \tag{2.17}$$

where $\delta_c = \inf\{\mu(\lambda) - \Re(z) : z \in \sigma(\mathcal{A}) \setminus \{\mu(\lambda)\}\} > 0$ is the spectral gap of the operator $\mathcal{A}$, and m_c is the invariant measure of Φ_t^c.

The exponential decay property of the FK operator Φ_t^c in the above proposition allows us to establish the existence of invariant measure m_c of Φ_t^c from a simple initial measure m (uniform or Gaussian) after long enough evolution. Since m_c is the invariant measure of Φ_t^c, for any $\phi \in S$, we have

$$\int_{\mathcal{D}} \phi dm_c = \left(\int_{\mathcal{D}} Q_t^c 1 dm_c\right)^{-1} \int_{\mathcal{D}} Q_t^c \phi dm_c. \tag{2.18}$$

This provides us a practical approach to compute the principal eigenvalue of Q_t^c by evaluating $\int_{\mathcal{D}} Q_t^c 1 dm_c$.

2.3. Numerical discretization and resampling techniques. For the time interval $[0, MT]$, let M denote the number of iterations, let H denote the number of discretization intervals of time in each iteration, and let $\Delta t = T/H$. At time $t_i = i\Delta t$ in one iteration, we can define the transform of random variables by the following formula:

$$\mathbf{Y}_i = \mathbf{X}_i + \mathbf{b}(\mathbf{X}_i)\Delta t + \sqrt{2\kappa\Delta t}\boldsymbol{\omega}_i, \tag{2.19}$$

where $\{\omega_i\}$ are independent and identically distributed (i.i.d.) d-dimensional standard Gaussian random variables which are independent of X_i. This transform represents a one-step Euler–Maruyama discretization scheme for process $\mathbf{X}_s^{T,0,\boldsymbol{x}}$ at time $s = T - i\Delta t$ which follows the SDE system (2.12). Then the one-step evolution operator $Q_i^{\Delta t}$ will be defined as follows:

$$Q_i^{\Delta t}\phi(\boldsymbol{x}) = \mathbb{E}(\phi(\mathbf{Y_i})|\mathbf{X}_i = \boldsymbol{x}), \quad \phi \in S. \tag{2.20}$$

The evolution operator $Q_i^{\Delta t}$ describes how the values of a given function evolve in L_2 sense over one time step Δt. One can easily verify that

$$||Q_i^{\Delta t} - e^{\Delta t\mathcal{L}}||_{L^2} \leq C_Q(\Delta t)^2, \tag{2.21}$$

where the operator $\mathcal{L}$ refers to (2.10), and C_Q is a positive constant [20]. Especially when $\boldsymbol{b} = 0$, $Q_{t_i}^{\Delta t} = e^{\Delta t\mathcal{L}}\ \forall\ i$. In addition, we can define the approximation operator for Q_t^c in (2.15). For instance, if we choose the right-point rectangular rule, we obtain that for any $m \in \mathcal{P}(\mathcal{D})$ and $\phi \in S$,

$$m(Q_i^{\Delta t}e^{\Delta t\mathcal{C}}\phi) = \mathbb{E}\Big(\phi(\mathbf{Y}_i)\exp\left(c(\mathbf{Y}_i)\Delta t\right)|\mathbf{X}_i \sim m\Big), \quad i = 1, 2, \ldots, H. \tag{2.22}$$

The time discretization for the FK semigroup (2.16) reads

$$\Phi_i^{\mathcal{C},\Delta t}(m)(\phi) = \frac{m(Q_i^{\Delta t}e^{\Delta t\mathcal{C}}\phi)}{m(Q_i^{\Delta t}e^{\Delta t\mathcal{C}}1)}, \quad i = 1, 2, \ldots, H. \tag{2.23}$$

Copyright © by SIAM and ASA. Unauthorized reproduction of this article is prohibited.

Downloaded 05/24/25 to 128.195.71.97 . Redistribution subject to SIAM license or copyright; see https://epubs.siam.org/terms-privacy

It is not practical to compute the closed-form solution of the evolution of the probability measure in (2.23). So we try to approximate the evolution of the probability measure in another way by an N-interacting particle system (N-IPS) [21]. Now we denote $\mathcal{K}^{\Delta t,i} = Q_i^{\Delta t} e^{\Delta t \mathcal{C}(t_i)}$ and define $\mathcal{K}^{\Delta t} = \mathcal{K}^{\Delta t,H}\mathcal{K}^{\Delta t,H-1}\cdots\mathcal{K}^{\Delta t,1}$.

$$\Phi^{\mathcal{K}^{\Delta t,i}}(m)(\phi) = \frac{m(\mathcal{K}^{\Delta t,i}\phi)}{m(\mathcal{K}^{\Delta t,i}1)}, \quad i = 1,2,\ldots,H, \tag{2.24}$$

is the FK semigroup associated with the operator $\mathcal{K}^{\Delta t,i}$.

Proposition 2.2 (Lemma 3.6 in [15]). *For any operators $\mathcal{A}$, $\mathcal{B}$ in $\mathcal{L}(L^2(\mathcal{D}))$, $\Phi^{\mathcal{A}\mathcal{B}} = \Phi^{\mathcal{B}}\Phi^{\mathcal{A}}$.*

According to Proposition 2.2, we have that

$$\Phi^{\mathcal{K}^{\Delta t}} = \prod_{i=0}^{H-1} \Phi^{\mathcal{K}^{\Delta t,H-i}} = \Phi^{\mathcal{K}^{\Delta t,1}}\Phi^{\mathcal{K}^{\Delta t,2}}\cdots\Phi^{\mathcal{K}^{\Delta t,H}}. \tag{2.25}$$

Suppose a Markov process $(\Theta, (\mathcal{F}_M)_{M\geq 0}, (\boldsymbol{\xi}^M)_{M\geq 0}, \mathbb{P})$ is defined in the product space $(\mathcal{D})^N$. By an N-IPS, we can approximate any initial probability measure $m_0 = m$ as

$$P(\boldsymbol{\xi}^0 \in d\boldsymbol{z}) = \prod_{l=1}^{N} m_0(dz^l). \tag{2.26}$$

Then according to [21] and denoting $\boldsymbol{\xi}^{M-1} = \boldsymbol{x}$, we evolve the N-IPS according to

$$P\left(\boldsymbol{\xi}^M \in d\boldsymbol{z} | \boldsymbol{\xi}^{M-1}\right) = \prod_{l=1}^{N} \Phi^{\mathcal{K}^{\Delta t}}\left(\frac{\sum_{i=1}^N \delta_{x^i}}{N}\right)(dz^l) = \prod_{l=1}^{N}\left(\prod_{j=0}^{H-1}\Phi^{\mathcal{K}^{\Delta t,H-j}}\right)\left(\frac{\sum_{i=1}^N \delta_{x^i}}{N}\right)(dz^l), \tag{2.27}$$

where N denotes the number of particles, vector $\boldsymbol{x} = (x^1,\ldots,x^N)^T$, and M denotes the iteration number of the probability measure's evolution by the FK semigroup defined in (2.23). Following equation (2.27), we compute each iteration of the evolution of N-IPS step by step from $\boldsymbol{\xi}^0$. And each iteration step will be divided into H small steps, and we denote $\boldsymbol{\xi}_i^M = (\xi_i^{1,M},\ldots,\xi_i^{N,M})$ as $\boldsymbol{\xi}^M$ after ith small steps ($i = 0,1,\ldots,H$). During each iteration stage, we evolve the particles from $s = 0$ to $s = T$ in the SDE (2.12) by the evolution operator $\{Q_i^{\Delta t}\}_{i=0}^{H-1}$ and then resample these particles according to their weights which are determined by the potential function. Specifically, each particle in the system is updated by

$$\widetilde{\xi}_i^{l,M-1} = \xi_i^{l,M-1} + \boldsymbol{b}(\xi_i^{l,M-1})\Delta t + \sqrt{2\kappa\Delta t}\boldsymbol{\omega}_i^{l,M-1}, \quad l = 1,2,\ldots,N, \tag{2.28}$$

where $\{\boldsymbol{\omega}_i^{l,M-1}\}$ are i.i.d. standard d-dimensional Gaussian random variables. Then by following the FK semigroup, we compute each particle's weight $w_i^{l,M-1}$ by (2.29), resample it according to the multinomial distribution of the particles' weights, and then obtain $\boldsymbol{\xi}_{i+1}^{M-1}$.

$$w_i^{l,M-1} = \frac{\exp\left(c(\widetilde{\xi}_i^{l,M-1})\Delta t\right)}{\sum_{l=1}^N \exp\left(c(\widetilde{\xi}_i^{l,M-1})\Delta t\right)}, \quad l = 1,2,\ldots,N. \tag{2.29}$$

Copyright © by SIAM and ASA. Unauthorized reproduction of this article is prohibited.

The whole evolution process of N-IPS from 0 to MT can be seen from Algorithm 2.1. The restriction step in this algorithm is the positional restriction back to the domain $\mathcal{D}$ for the particles that are about to escape from the range of $\mathcal{D}$ during the evolution process. For example, under the periodic velocity field condition in $\mathcal{D} = [0, \frac{1}{\Delta k}]^d$, we update the particle position in each dimension by $x \leftarrow mod(x, \frac{1}{\Delta k})$.

After obtaining the particles' $\boldsymbol{\xi}_0^M$ empirical distribution, we compute $\mu_{\Delta t}^M(\lambda)$. At the Mth iteration stage, we first define the change of the mass as follows:

$$e_{i,M}^N = N^{-1} \sum_{l=1}^{N} \exp(c(\widetilde{\xi}_i^{l,M})\Delta t). \tag{2.30}$$

Then, we compute the μ approximation as

$$\mu_{\Delta t}^M(\lambda) = (H\Delta t)^{-1} \sum_{i=0}^{H-1} \log\left(N^{-1} \sum_{l=1}^{N} \exp(c(\widetilde{\xi}_i^{l,M})\Delta t) \right). \tag{2.31}$$

We know that the particles' $\boldsymbol{\xi}_0^M$ empirical distribution will weakly converge to the distribution $\Phi_n^{\mathcal{K}^{\Delta t}}(m_0)$ as N approaches infinity. Therefore, we can use $\mu_{\Delta t}^M(\lambda)$ as an approximation to $\mu(\lambda)$. Equation (2.31) is the discrete version of the following formula:

$$\mu^M(\lambda) = \frac{1}{T} \int_{(M-1)T}^{MT} \ln \mathbb{E}\left[\exp(c(X_s^{MT,0,\boldsymbol{x}}))\right] ds. \tag{2.32}$$

Compared to using the FK formula (2.13) directly, the first thing we need to realize is that the limits of (2.13) and (2.31) are equivalent due to the ergodicity. In (2.31), only the states during the final iteration, i.e., Mth iteration, are taken into account in the computation of $\mu_{\Delta t}^M$. In contrast, directly applying the FK formula (2.13) requires accounting for the whole evolution process, i.e., from $t = 0$ to $t = MT$, which is numerically unstable in the long-time computation. Algorithm 2.1 shows the entire evolution process.

3. Convergence analysis.

In this section, we demonstrate the convergence of the IPM in computing the KPP front speed of the stationary and isotropic Gaussian random fields with discrete spectrum defined as in (2.1). If we consider the system in $\mathbb{R}^d$ directly, our particle approach is easy to implement for computation. However, due to the lack of spectral gap conditions and bounded settings, convergence analysis is difficult to carry out directly. Since the random velocity field $\boldsymbol{v}(\boldsymbol{x}, \omega)$ in this setting always has period $1/\Delta k$, the motion of the particle can be considered in the torus $\mathcal{D} = [0, 1/\Delta k]^d$. In [15], the authors gave the convergence analysis of the cases with deterministic velocity fields. Due to each random realization, the realized velocity field will perform as a deterministic case, so we divide the analysis into four parts. The first part studies the approximation of the random field with a discrete spectrum by the random Fourier method. The second part studies the error estimate of an operator splitting method to approximate the evolution of parabolic operators. The third part studies the error estimate of the IPM in μ computation. The fourth part studies the error estimate in computing μ via the random Fourier method.

Downloaded 05/24/25 to 128.195.71.97 . Redistribution subject to SIAM license or copyright; see https://epubs.siam.org/terms-privacy

Copyright © by SIAM and ASA. Unauthorized reproduction of this article is prohibited.

Algorithm 2.1. Genetic algorithm for computing $\mu^n_{\Delta t}(\lambda)$.

Require: Input: velocity field $\boldsymbol{v}(\boldsymbol{x},\omega)$, potential $c(\boldsymbol{x},\omega)$, initial probability measure m_0, Monte Carlo number N, iteration number M, time step Δt, generation life span $T = H\Delta t$ and $t_i = i\Delta t,\ 0 \le i \le H$ (mutation number).

Generate N i.i.d. m_0-distributed random variables $\boldsymbol{\xi}_0^0 = (\xi_0^{1,0}, \dots, \xi_0^{N,0})$ on $\mathcal{D}$
for $j = 1 : M$ **do**
  for $i = 0 : H-1$ **do**
    Generate N i.i.d. standard Gaussian random variables.
    Compute $\tilde{\boldsymbol{\xi}}_i^{j-1} = (\tilde{\xi}_i^{1,j-1}, \dots, \tilde{\xi}_i^{N,j-1})$ from $\boldsymbol{\xi}_i^{j-1}$ by (2.28).
    Restrict $\tilde{\boldsymbol{\xi}}_i^{j-1}$ on $\mathcal{D}$ by imposing boundary condition (not needed on $\mathbb{R}^d$).
    Compute pointwise fitness array $\boldsymbol{S} \overset{\text{def}}{=} (\exp(c^1\Delta t), \dots, \exp(c^N\Delta t))$, where $c^k = c(\tilde{\xi}_i^{k,j-1}, \omega),\ 1 \le k \le N$.
    Define weight array $\boldsymbol{w} = (w_i^{1,j-1}, \dots, w_i^{N,j-1}) \overset{\text{def}}{=} \boldsymbol{S}/sum(\boldsymbol{S})$ via fitness, and compute mutationwise mean particle fitness growth rate (PFGR): $\boldsymbol{E}_{j,i} \overset{\text{def}}{=} \log(mean(\boldsymbol{S}))/\Delta t$
    Resample $\tilde{\boldsymbol{\xi}}_i^{j-1}$ by $\boldsymbol{w}$-parameterized multinomial distribution to get $\boldsymbol{\xi}_{i+1}^{j-1}$.
  end for
  Generationwise mean PFGR: $\mu^j_{\Delta t}(\lambda) \overset{\text{def}}{=} H^{-1}\sum_{i=0}^{H-1}(\boldsymbol{E}_{j,i})$ and set $\boldsymbol{\xi}_0^j = \boldsymbol{\xi}_H^{j-1}$.
end for

Ensure: Output $\mu^M_{\Delta t}(\lambda)$ and approximately time-invariantly distributed $\boldsymbol{\xi}_0^M$.

3.1. Approximating Gaussian random field with a prescribed discrete spectrum by random Fourier method.

In this subsection, we first represent the linearized corrector KPP equation (2.8) in a nonautonomous parabolic equation in each iteration,

$$q_t = \kappa\Delta_{\boldsymbol{x}} q + \boldsymbol{b}(\boldsymbol{x},\omega)\cdot\nabla_{\boldsymbol{x}} q + c(\boldsymbol{x},\omega)q, \quad \boldsymbol{x} = (x_1,\dots,x_d)^T \in \mathcal{D}, \quad t \in [0,T], \tag{3.1}$$

with the initial condition $q(\boldsymbol{x},0) = q_0$. Here $\boldsymbol{b}(\boldsymbol{x},\omega) = -2\kappa\lambda\boldsymbol{e} + \boldsymbol{v}$, $c(\boldsymbol{x},\omega) = \kappa\lambda^2 - \lambda\boldsymbol{v}\cdot\boldsymbol{e} + f'(0)$. For Gaussian random field $\boldsymbol{v}(\boldsymbol{x},\omega)$ defined by (2.1), it is fully characterized by its mean and covariance function. For each realization of the random field, our strategy is to generate an approximation $\tilde{\boldsymbol{v}}(\boldsymbol{x})$ of the random velocity field, $\boldsymbol{v}(\boldsymbol{x},\omega)$, with long-range correlation according to the correlation functions. Generated by the random Fourier method, $\tilde{\boldsymbol{v}}$ can be used with confidence to predict some important scaling laws and can simulate the spreading of particles accurately and efficiently. We use the simplest tracer statistic of the sort to measure the spreading of the particles. In the SDE system (2.12),

$$d\boldsymbol{X}_s = \boldsymbol{b}(\boldsymbol{X}_s,\omega)ds + \sqrt{2\kappa}d\mathbf{w}(s), \quad \boldsymbol{X}_0 = \boldsymbol{x}', \tag{3.2}$$

where $\mathbf{w}(s)$ is d-dimensional standard Brownian motion, and its variance at time s in each dimensional is $2\kappa s$. The stochastic drift term $\boldsymbol{b}(\boldsymbol{X}_s,\omega)$ is independent of $\mathbf{w}(s)$, so their variances are additional. We denote the deterministic part of $\boldsymbol{b}(\boldsymbol{X}_s,\omega)$ as $\boldsymbol{b}_0(\boldsymbol{X}_s)$. Since $\boldsymbol{v}$ is mean zero and stationary, we have $\langle\boldsymbol{b}(\boldsymbol{X}_s,\omega)\rangle = \boldsymbol{b}_0(\boldsymbol{X}_s)$, and the covariance function between two points $\boldsymbol{X}_s, \boldsymbol{X}_s + \boldsymbol{x}$ can be computed by

Copyright © by SIAM and ASA. Unauthorized reproduction of this article is prohibited.

Downloaded 05/24/25 to 128.195.71.97 . Redistribution subject to SIAM license or copyright; see https://epubs.siam.org/terms-privacy

$$\begin{aligned}\langle(\boldsymbol{b}(\boldsymbol{X}_s,\omega)-\boldsymbol{b}_0(\boldsymbol{X}_s))\cdot(\boldsymbol{b}(\boldsymbol{X}_s+\boldsymbol{x},\omega)-\boldsymbol{b}_0(\boldsymbol{X}_s+\boldsymbol{x}))\rangle &= \langle\boldsymbol{v}(\boldsymbol{X}_s,\omega)\cdot\boldsymbol{v}(\boldsymbol{X}_s+\boldsymbol{x},\omega)\rangle \\ &= R(\boldsymbol{x}).\end{aligned} \tag{3.3}$$

Here $\langle\cdot\rangle$ denotes the average over probability space induced by ω, and $R(\boldsymbol{x})$ denotes the two-point correlation function of $\boldsymbol{v}$. Since $\boldsymbol{v}$ is isotropic, the correlation function $R(\boldsymbol{x})$ admits the following representations:

$$R(\boldsymbol{x}) = R(x) = \langle\boldsymbol{v}(x_0,\omega)\cdot\boldsymbol{v}(x_0+x,\omega)\rangle = 2\sum_{j=0}^{+\infty}\Delta k\cos(2\pi k_j r)E(k_j),\ \text{(1D)}, \tag{3.4}$$

$$R(\boldsymbol{x}) = \langle\boldsymbol{v}(\boldsymbol{x}_0,\omega)\cdot\boldsymbol{v}(\boldsymbol{x}_0+\boldsymbol{x},\omega)\rangle = 2\sum_{j=0}^{+\infty}\Delta k J_0(2\pi k_j r)E(k_j),\ \text{(2D)}, \tag{3.5}$$

$$R(\boldsymbol{x}) = \langle\boldsymbol{v}(\boldsymbol{x}_0,\omega)\cdot\boldsymbol{v}(\boldsymbol{x}_0+\boldsymbol{x},\omega)\rangle = 2\sum_{j=0}^{+\infty}\Delta k\frac{\sin(2\pi k_j r)}{2\pi k_j r}E(k_j),\ \text{(3D)}, \tag{3.6}$$

where $E(k)$ is a given energy spectral density, $k_j = j\Delta k$, $J_0(\cdot)$ is the Bessel function of the first kind, and $r = ||\boldsymbol{x}||_2$. We know that the mean square displacement is also completely determined by the correlation function $R(\boldsymbol{x})$. So, the important thing is that the generated velocity field's correlation function $\tilde{R}(\boldsymbol{x})$ should be an approximation to the true random velocity field's correlation function $R(\boldsymbol{x})$. Following the random Fourier method mentioned in section 2.1, to make it accurate at low frequency, we would require $E(k)$ to satisfy the following properties:

P1. $E(k)$ is integrable and has finite moments. Since $E(k)$ is nonnegative, this also implies $E(k)\in L^1(\mathbb{R})$.
P2. $E(k)$ is finite at zero point, i.e., $E(0)<+\infty$.
P3. $E(k), E'(k), E''(k)$ are all bounded a.e.
P4. Let $g(y) = 2\sum_{j=y}^{+\infty}E(k_j)\Delta k$. For all $C_g>0$, $\exists y_0\in\mathbb{N}^+$, $\forall y>y_0$ and $y\in\mathbb{N}^+, g(y)<C_g/y^2$, i.e., $g(y)$ decay to 0 at least as $O(y^{-2})$ as y goes to infinity.

From properties P1 to P4, we can also imply that the correlation function $R(\boldsymbol{x})$ is always finite. Then by comparing the two correlation functions (2.6) and (2.7), we see that the error between the two velocity fields' correlation function is the truncation error. In other words, the error is related to the number of Fourier mode N_F (or the length of truncated frequency interval $k_{max} = (N_F+\frac{1}{2})\Delta k$). For a specific N_F and Δk, the truncation error e_R in 1D cases can be represented by

$$\begin{aligned}e_R(N_F) &= \left|2\sum_{j=0}^{\infty}\cos(2\pi k_j x)E(k_j)\Delta k - 2\sum_{j=0}^{N_F}\cos(2\pi k_j x)E(k_j)\Delta k\right| \\ &= 2\sum_{j=N_F+1}^{\infty}|\cos(2\pi k_j x)E(k_j)\Delta k| < g(N_F+1).\end{aligned} \tag{3.7}$$

Lemma 3.1. *The error, e_R, between the corresponding correlation functions of two velocity fields, $\boldsymbol{v}$ and $\tilde{\boldsymbol{v}}$, decays to zero at a convergence rate of $O((N_F)^{-2})$; i.e., for any $C_g>0$, $\exists N_{F_0}\in N^+, \forall N_F>N_{F_0}$, and $N_F\in N^+$, s.t.*

Downloaded 05/24/25 to 128.195.71.97 . Redistribution subject to SIAM license or copyright; see https://epubs.siam.org/terms-privacy

Copyright © by SIAM and ASA. Unauthorized reproduction of this article is prohibited.

$$e_R(N_F) \le \frac{C_g}{(N_F)^2}. \tag{3.8}$$

Proof. The truncation error, e_R, will be related to the performance of $E(k)$ at large frequency. From the properties P1 to P4 we mentioned above, for any $C_g > 0$, with sufficient large N_F, we have

$$e_R(N_F) \le g(N_F+1) < \frac{C_g}{(N_F+1)^2} < \frac{C_g}{(N_F)^2}. \tag{3.9}$$

■

For 2D and 3D cases, we can follow the same idea and get similar estimates. In [15], the author assumed that the deterministic parts $\boldsymbol{b}_0(\boldsymbol{x})$ and $c_0(\boldsymbol{x})$ satisfy $||\boldsymbol{b}_0(\boldsymbol{x})||_{L^2} \le M_1$, $|c_0(\boldsymbol{x})| \le M_2$, $||\nabla_{\boldsymbol{x}} c_0(\boldsymbol{x})||_{L^2} \le M_3$, and $||\Delta_{\boldsymbol{x}} c_0(\boldsymbol{x})||_{L^2} \le M_4$. Now we analyze these assumptions for the random velocity field $\boldsymbol{v}$ in a torus $\mathcal{D}$, using $\tilde{\boldsymbol{v}}$ as an approximation of $\boldsymbol{v}$ in practical experiments.

Lemma 3.2. *For a probability p close to 1, the term $||\boldsymbol{b}(\boldsymbol{x},\omega)||_{L^2}$ corresponding to the random velocity field mentioned above has its upper bound $\tilde{M}_1$, so that*

$$P(||\boldsymbol{b}(\boldsymbol{x},\omega)||_{L^2} < \tilde{M}_1) > p. \tag{3.10}$$

The terms $|c(\boldsymbol{x})|, ||\nabla_{\boldsymbol{x}} c(\boldsymbol{x})||_{L^2}, ||\Delta_{\boldsymbol{x}} c(\boldsymbol{x})||_{L^2}$ can also find their corresponding upper bounds $\tilde{M}_2, \tilde{M}_3, \tilde{M}_4$.

The Plancherel theorem and Markov inequality have been used in our proof. The detailed proof can be found in Appendix B.

3.2. Approximating parabolic evolution by operator splitting. We recall the nonautonomous parabolic equation (3.1) and use $\tilde{\boldsymbol{v}}$ as an approximation to $\boldsymbol{v}$. From the notation defined in (2.10) and (2.11), we can define

$$\mathcal{A}(\boldsymbol{x},\omega) = \mathcal{L}(\boldsymbol{x},\omega) + \mathcal{C}(\boldsymbol{x},\omega), \tag{3.11}$$

where $\mathcal{L}(\boldsymbol{x},\omega) = \kappa\Delta_{\boldsymbol{x}} + \boldsymbol{b}(\boldsymbol{x},\omega)\cdot\nabla_{\boldsymbol{x}}$ and $\mathcal{C}(\boldsymbol{x},\omega) = c(\boldsymbol{x},\omega)$. Similarly, we can define $\tilde{\mathcal{A}}, \tilde{\mathcal{L}}$ and $\tilde{\mathcal{C}}$ to be the corresponding operators for $\tilde{\boldsymbol{v}}$. We know that in each realization, the velocity field $\tilde{\boldsymbol{v}}$ is realized as a time-independent and space-periodic field. Then the operator $\tilde{\mathcal{A}}(\boldsymbol{x},\omega_i) = \tilde{\mathcal{A}}(\boldsymbol{x})$ has a real, isolated principal eigenvalue [8]. Here we treat $\mathcal{A}(\boldsymbol{x},\omega)$ as the deterministic part $\tilde{\mathcal{A}}$ with a small random perturbation (caused by the remainder of the velocity field $\boldsymbol{v} - \tilde{\boldsymbol{v}}$). Following the perturbation theory in [10], for the spectrum $\Sigma(\tilde{\mathcal{A}})$ of the deterministic infinite system $\tilde{\mathcal{A}}$ mentioned above, using the spectral gap condition, we can first separate it into $\Sigma'(\tilde{\mathcal{A}})$ and $\Sigma''(\tilde{\mathcal{A}})$ where $\Sigma'(\tilde{\mathcal{A}})$ is a finite system.

Proposition 3.1. *The change in a finite system $\Sigma'(\tilde{\mathcal{A}})$ of the eigenvalues of a closed operator $\tilde{\mathcal{A}}$ is small (in the sense of Proposition A.1) when $\tilde{\mathcal{A}}$ is subject to a small perturbation in the sense of generalized convergence.*

Proposition 3.1 guarantees the existence of $\mu(\lambda)$ of $\mathcal{A}$ when it is treated as the original deterministic operator $\tilde{\mathcal{A}}$ subject to a relatively small random perturbation in each realization. The detailed explanation of Proposition 3.1 can be found in Appendix A. Then we define a solution operator $\mathcal{U}(t,q) : \mathcal{U}(t,s)q(\cdot,s) = q(\cdot,t)$ corresponding to the nonautonomous parabolic equation (3.1). This solution operator $\mathcal{U}(t,s)$ maps the solution of equation (3.1) at time point s to the solution at time point t. It is easy to verify the following:

Copyright © by SIAM and ASA. Unauthorized reproduction of this article is prohibited.

Downloaded 05/24/25 to 128.195.71.97 . Redistribution subject to SIAM license or copyright; see https://epubs.siam.org/terms-privacy

1. $\mathcal{U}(s,s) = Id \ \forall\ s \geq 0$;
2. $\mathcal{U}(t,r) \circ \mathcal{U}(r,s) = \mathcal{U}(t,s)\ \forall\ t \geq r \geq s \geq 0$;
3. $\frac{d}{dt}\mathcal{U}(t,s)q_0 = \mathcal{A}(\boldsymbol{x},\omega)\ \mathcal{U}(t,s)q_0\ \forall\ t \geq s \geq 0, q_0 \in L^2(\mathcal{D})$.

The solution operator provides us an approach for studying the parabolic equation (3.1). The principal eigenvalue of the parabolic operator $\mathcal{A}$ can be given by the principal eigenvalue of the solution operator $\mathcal{U}(T,0)$. Although the principal eigenvalue of $\mathcal{U}(T,0)$ exists and is real [8], it is difficult to have it in closed form for this operator. Therefore, we adopt an operator splitting method to approximate $\mathcal{U}(T,0)$.

We divide the time interval into H equal subintervals, set $\Delta t = \frac{T}{H}$, $t_i = i\Delta t$, and consider the following parabolic equation during a time subinterval:

$$q_t = \kappa \Delta_{\boldsymbol{x}} q + \boldsymbol{b}(\boldsymbol{x},\omega) \cdot \nabla_{\boldsymbol{x}} q + c(\boldsymbol{x},\omega) q, \quad t_i < t \leq t_{i+1}, \quad i \geq 0. \tag{3.12}$$

Then we can represent the corresponding solution operator as

$$q(t) = e^{(t-t_i)(\mathcal{L}+\mathcal{C})} \prod_{h=0}^{i-1} e^{\Delta t_h (\mathcal{L}+\mathcal{C})} q_0, \quad t_i \leq t < t_{i+1}. \tag{3.13}$$

Here $\Delta t_h = \Delta t = \frac{T}{H}$, just to emphasize that it corresponds to the hth time subinterval. Furthermore, after applying the first-order Lie–Trotter operator splitting method to get an approximation to the solution operator defined in (3.13), we obtain

$$q(t) = e^{(t-t_i)\mathcal{L}} e^{(t-t_i)\mathcal{C}} \prod_{h=0}^{i-1} e^{\Delta t_h \mathcal{L}} e^{\Delta t_h \mathcal{C}} q_0, \quad t_i \leq t < t_{i+1}. \tag{3.14}$$

It has been proved that the solution operator $\prod_{h=0}^{H-1} e^{\Delta t_h \mathcal{L}} e^{\Delta t_h \mathcal{C}}$ obtained by the first-order Lie–Trotter splitting method converges to the corresponding solution operator $\mathcal{U}(T,0)$ as $\Delta t \to 0$ in a certain operator norm (Theorem 3.4 in [15]). In the case when $\boldsymbol{b}(\boldsymbol{x},\omega)$ and $c(\boldsymbol{x},\omega)$ are uniformly Lipschitz in $\boldsymbol{x}$, the authors of [15] also provided the error estimate, which shows that the error of the principal eigenvalue obtained by the Lie–Trotter operator splitting method is at least $O((\Delta t)^{\frac{1}{2}})$.

3.3. Error estimate of particle method. For operator $\mathcal{A}$ defined in (3.11), we consider its corresponding FK operator $\Phi^{\mathcal{A}}$ with a probability measure m defined by

$$\Phi^{\mathcal{A}}(m)(\phi) = \frac{m(\mathcal{A}\phi)}{m(\mathcal{A}1)} \quad \forall \phi \in L^2(\mathcal{D}). \tag{3.15}$$

Moreover, we denote $\Phi^{\mathcal{A}}_M = (\Phi^{\mathcal{A}})^M$. It is easy to verify that the FK semigroup $\Phi^{\cdot}$ satisfies the property $\Phi^{\mathcal{A}\mathcal{B}} = \Phi^{\mathcal{B}}\Phi^{\mathcal{A}}\ \forall\ \mathcal{A},\mathcal{B} \in \mathcal{L}(L^2(\mathcal{D}))$.

Recall that the operator $\Phi^{\mathcal{K}^{\Delta t}}$ defined in (2.25) is constructed from the FK semigroup $\Phi^{\mathcal{K}^{\Delta t,i}}$ defined in (2.24) which corresponds to the operator $\mathcal{K}^{\Delta t,i}$. We show several important results to ensure the existence of an invariant measure for the discretized FK dynamics and give an error estimate for computing the principal eigenvalue of the parabolic operator $\tilde{\mathcal{A}}(\boldsymbol{x})$ defined as in (3.11).

Downloaded 05/24/25 to 128.195.71.97 . Redistribution subject to SIAM license or copyright; see https://epubs.siam.org/terms-privacy

Copyright © by SIAM and ASA. Unauthorized reproduction of this article is prohibited.

Downloaded 05/24/25 to 128.195.71.97 . Redistribution subject to SIAM license or copyright; see https://epubs.siam.org/terms-privacy

Proposition 3.2 (Theorem 3.7 in [15]). *There exists a probability measure $m^{\mathcal{K}}$ so that the operator $\mathcal{K}^{\Delta t}$ satisfies a uniform minorization and boundedness condition as follows:*

$$\theta m^{\mathcal{K}}(\phi) \le \mathcal{K}^{\Delta t}(\phi)(\boldsymbol{x}) \le \vartheta m^{\mathcal{K}}(\phi) \quad \forall\ \boldsymbol{x} \in \mathcal{D}, \quad \forall\ \phi \in L^2(\mathcal{D}), \tag{3.16}$$

where $0 < \theta < \vartheta$ are independent of Δt and ϕ. Moreover, when $\Delta t \to 0$, the limit operator is the exact solution operator $\mathcal{U}(T,0)$, which also satisfies this uniform minorization and boundedness condition.

Proposition 3.3 (Theorem 3.8 in [15]). *Suppose the minorization and boundedness conditions (3.16) hold. Then, $\Phi_M^{\mathcal{K}^{\Delta t}}$ admits an invariant measure $m_{\Delta t}$, whose density function is the eigenfunction of the operator $(\mathcal{K}^{\Delta t})^\star$, the adjoint operator of the solution operator $\mathcal{K}^{\Delta t}$. Moreover, for any initial distribution $m_0 \in \mathcal{P}(\mathcal{D})$, we have*

$$||\Phi_M^{\mathcal{K}^{\Delta t}}(m_0) - m_{\Delta t}||_{TV} \le 2\left(1 - \frac{\theta}{\vartheta}\right)^M, \tag{3.17}$$

where $||\cdot||_{TV}$ is the total variation norm, and $0 < \theta < \vartheta$ are the parameters defined in the minorization and boundedness conditions in (3.16). The estimate (3.17) is also true when changing $\mathcal{K}^{\Delta t}$ to the exact solution operator $\mathcal{U}(T,0)$.

Propositions 3.2 and 3.3 show that the operator $\mathcal{K}^{\Delta t}$ satisfies a uniform minorization and boundedness condition and then can guarantee that $\Phi_M^{\mathcal{K}^{\Delta t}}$ admits an invariant measure. The details of the proof can be found in [15, 19]. Then the principal eigenvalue of operator $\mathcal{K}^{\Delta t}$ satisfies the following relation:

$$e^{\mu_{\Delta t}(\lambda)T} = m_{\Delta t}\mathcal{K}^{\Delta t}1 = \Phi_M^{\mathcal{K}^{\Delta t}}(m_0)\mathcal{K}^{\Delta t}1 + \rho_M, \tag{3.18}$$

where $m_{\Delta t}$ and m_0 are just the probability measures mentioned in Proposition 3.3, T is the period in time, and ρ_M is $O(1-\frac{\theta}{\vartheta})^M$. Denote $m_{\Delta t}^h = \prod_{i=0}^{h-1} \Phi^{\mathcal{K}^{\Delta t, H-i}} m_{\Delta t}$, $1 \le h \le H$. Let $e_h = (m_{\Delta t}^h)(\mathcal{K}^{\Delta t, H-h}1)$ denote the changing of mass. Then, we have

$$e^{\mu_{\Delta t}(\lambda)T} = \prod_{h=1}^{H} e_h \quad \text{and} \quad \mu_{\Delta t}(\lambda) = \frac{1}{H\Delta t}\sum_{h=0}^{H-1} \log(e_h). \tag{3.19}$$

Then we represent an important result that gives the error analysis of computing the principal eigenvalue of $\mathcal{A}(t)$ using the particle method. Since the random fields we consider have an equispaced discrete spectrum, the following proposition remains valid.

Proposition 3.4 (Theorem 3.11 in [15]). *Suppose $\boldsymbol{b}(\boldsymbol{x})$ and $c(\boldsymbol{x})$ in $\mathcal{A}(\boldsymbol{x})$ are bounded, smooth, and periodic in each component of $\boldsymbol{x}$, and uniformly Hölder continuous in t. Let*

$$\mu_{\Delta t}^M(\lambda) = (H\Delta t)^{-1}\sum_{h=0}^{H-1} \log\left(N^{-1}\sum_{l=1}^{N} \exp(c(\widetilde{\xi}_h^{l,M-1})\Delta t)\right) \tag{3.20}$$

denote the approximate principal eigenvalue obtained by the N-IPS method, where $\widetilde{\xi}_h^{l,M-1}$, $h = 0,\dots,H-1$, $l = 1,\dots,N$, M is the iteration number, and $\Delta t = T/H$ is the time step. Let

Copyright © by SIAM and ASA. Unauthorized reproduction of this article is prohibited.

$\mu(\lambda)$ denote the principal eigenvalue of (2.8) defined in (2.13). Then, we have the following convergence result:

(3.21)
$$\lim_{N\to\infty}\frac{1}{H\Delta t}\sum_{h=0}^{H-1}\log\left(\frac{1}{N}\sum_{l=1}^{N}\exp(c(\widetilde{\xi}_h^{l,M-1})\Delta t)\right)=\mu(\lambda)+O\left(\left(1-\frac{\theta}{\vartheta}\right)^M\right)+O((\Delta t)^{\frac{1}{2}}),$$

where $0<\theta<\vartheta$ are the parameters defined in the minorization and boundedness conditions in (3.16).

The standing assumption in [15] is a deterministic periodic flow, while in this paper it is a random flow with an equispaced discrete spectrum. Since every random field realization at this point still has a period, Proposition 3.4 is still valid. As discussed in (2.31), we substitute the long-time limit (2.13) with the final state limit. This is due to the ergodicity nature of both the original system and the discrete system. Then the final error estimate in Proposition 3.4 consists of the difference of ergodic limits between continuous and discrete systems (generally a cell problem $O(\Delta t)$) and the difference between final state and ergodic limit in the discrete system (geometrically decreasing).

3.4. Error estimate in computing μ via random Fourier method. Here we will give some statistical error analysis on the solution operator. By the approximation to random velocity field and the operator splitting method, it has the following error in approximating the solution operator $\mathcal{U}(T,0)$ in L^2 operator norm:

$$e_{op}\overset{\text{def}}{=}\left\|\mathcal{U}(T,0)q-\prod_{h=1}^{H}e^{\Delta t_h\tilde{\mathcal{L}}(\boldsymbol{x},\omega)}e^{\Delta t_h\tilde{\mathcal{C}}(\boldsymbol{x},\omega)}q\right\|_{L^2}. \tag{3.22}$$

Here $\tilde{\mathcal{L}}$ and $\tilde{\mathcal{C}}$ denote the corresponding operators in (3.11) of $\tilde{\boldsymbol{v}}$. We can separate this error into three parts and define them by

$$e_1\overset{\text{def}}{=}\left\|\mathcal{U}(T,0)q-\prod_{h=1}^{H}e^{\Delta t_h\mathcal{A}(\boldsymbol{x},\omega)}q\right\|_{L^2}, \tag{3.23}$$

$$e_2\overset{\text{def}}{=}\left\|\prod_{h=1}^{H}e^{\Delta t_h\mathcal{A}(\boldsymbol{x},\omega)}q-\prod_{h=1}^{H}e^{\Delta t_h\mathcal{L}(\boldsymbol{x},\omega)}e^{\Delta t_h\mathcal{C}(\boldsymbol{x},\omega)}q\right\|_{L^2}, \tag{3.24}$$

$$e_3\overset{\text{def}}{=}\left\|\prod_{h=1}^{H}e^{\Delta t_h\mathcal{L}(\boldsymbol{x},\omega)}e^{\Delta t_h\mathcal{C}(\boldsymbol{x},\omega)}q-\prod_{h=1}^{H}e^{\Delta t_h\tilde{\mathcal{L}}(\boldsymbol{x},\omega)}e^{\Delta t_h\tilde{\mathcal{C}}(\boldsymbol{x},\omega)}q\right\|_{L^2}. \tag{3.25}$$

Here e_1, e_2, and e_3 correspond to the error caused by solution operator (3.13), the Lie–Trotter operator splitting method, and using the random Fourier method. Then by triangle inequality, we can get that

$$e_{op}\le e_1+e_2+e_3. \tag{3.26}$$

Copyright © by SIAM and ASA. Unauthorized reproduction of this article is prohibited.

Downloaded 05/24/25 to 128.195.71.97 . Redistribution subject to SIAM license or copyright; see https://epubs.siam.org/terms-privacy

Downloaded 05/24/25 to 128.195.71.97 . Redistribution subject to SIAM license or copyright; see https://epubs.siam.org/terms-privacy

Proposition 3.5. *Suppose $\boldsymbol{b}(\boldsymbol{x},\omega)$ and $c(\boldsymbol{x},\omega)$ in the operator $\mathcal{A}=\mathcal{L}+\mathcal{C}$ are bounded and smooth in a bounded domain $\mathcal{D}$; then there exists γ_1 large enough and $\gamma_2>0$, such that*

$$||\kappa\Delta_{\boldsymbol{x}}+(c(\boldsymbol{x},\omega)-\gamma_1)\boldsymbol{v}||_{L^2}\geq\hat{C}_1(||\Delta_{\boldsymbol{x}}\boldsymbol{v}||_{L^2}+||\boldsymbol{v}||_{L^2}), \tag{3.27}$$

$$||[\mathcal{L},\mathcal{C}]\boldsymbol{v}||_{L^2}\leq\hat{C}_2||(\mathcal{L}-\gamma_2)\boldsymbol{v}||_{L^2}^{\frac{1}{2}}||\boldsymbol{v}||_{L^2}^{\frac{1}{2}}, \tag{3.28}$$

where $\hat{C}_1$ and $\hat{C}_2$ are constants and independent of $\boldsymbol{x}$ and ω.

A detailed explanation can be found in [15] and Lemmas 3.2 and 3.3. From Lemma 3.2, we can derive the upper bounds for $||\boldsymbol{b}(\boldsymbol{x},\omega)||_{L^2}$, $|c(\boldsymbol{x},\omega)|$, $||\nabla_{\boldsymbol{x}}c(\boldsymbol{x},\omega)||_{L^2}$, $||\Delta_{\boldsymbol{x}}c(\boldsymbol{x},\omega)||_{L^2}$ for a probability p close to 1. Following the same approach, we can obtain the corresponding upper bounds for $||\tilde{\boldsymbol{b}}(\boldsymbol{x},\omega)||_{L^2}$, $|\tilde{c}(\boldsymbol{x},\omega)|$, $||\nabla_{\boldsymbol{x}}\tilde{c}(\boldsymbol{x},\omega)||_{L^2}$, $||\Delta_{\boldsymbol{x}}\tilde{c}(\boldsymbol{x},\omega)||_{L^2}$.

Lemma 3.3. *We can construct γ by these upper bounds, and the operators $\mathcal{A}-\gamma,\tilde{\mathcal{A}}-\gamma$ will both satisfy the requirements in Proposition 3.5 with probability greater than p.*

Proof. From the analysis in Appendix B, we have obtained the upper bounds corresponding to the terms comprising $\boldsymbol{b}(\boldsymbol{x},\omega)$ and $c(\boldsymbol{x},\omega)$. So, for any probability p close to 1, we can find the number $\tilde{M}_1$, $\tilde{M}_1'$ such that

$$P(||\boldsymbol{b}(\boldsymbol{x},\omega)||_{L^2}<\tilde{M}_1)>p\quad\text{and}\quad P(||\tilde{\boldsymbol{b}}(\boldsymbol{x},\omega)||_{L^2}<\tilde{M}_1')>p. \tag{3.29}$$

Then we take $M_1^*=\max(\tilde{M}_1,\tilde{M}_1')$. Following the same idea, we can get the upper bounds M_2^*,M_3^*, and M_4^* which correspond to $|c(\boldsymbol{x},\omega)|,||\nabla_{\boldsymbol{x}}c(\boldsymbol{x},\omega)||_{L^2}$ and $||\Delta_{\boldsymbol{x}}c(\boldsymbol{x},\omega)||_{L^2}$. Following the idea in [15] and Lemmas 3.2 and 3.3, for $(\boldsymbol{b}(\boldsymbol{x},\omega),\ c(\boldsymbol{x},\omega))$ and $(\tilde{\boldsymbol{b}}(\boldsymbol{x},\omega),\ \tilde{c}(\boldsymbol{x},\omega))$, we can find, respectively, (γ_1,γ_2) and $(\tilde{\gamma}_1,\tilde{\gamma}_2)$. We take $\tilde{\gamma}=\max(\gamma_1,\gamma_2,\tilde{\gamma}_1,\tilde{\gamma}_2)$ and take $\gamma=\tilde{\gamma}+M_2^*$ where $|c(\boldsymbol{x},\omega)|<M_2^*$ and $|\tilde{c}(\boldsymbol{x},\omega)|<M_2^*$ are satisfied with probability greater than p. Let $\mathcal{U}_\gamma(t,s)=e^{-\gamma(t-s)}\mathcal{U}(t,s)$ be the solution operator which corresponds to the parabolic equation (3.12) with $\mathcal{A}_\gamma=\mathcal{A}_\gamma(\boldsymbol{x},\omega)=\mathcal{A}(\boldsymbol{x},\omega)-\gamma$, $\mathcal{L}_\gamma=\mathcal{L}_\gamma(\boldsymbol{x},\omega)=\mathcal{L}(\boldsymbol{x},\omega)-\tilde{\gamma}$, and $\mathcal{C}_\gamma=\mathcal{C}_\gamma(\boldsymbol{x},\omega)=\mathcal{C}(\boldsymbol{x},\omega)-M_2^*$. Similarly, for $\tilde{\mathcal{A}}(\boldsymbol{x},\omega),\tilde{\mathcal{L}}(\boldsymbol{x},\omega)$, and $\tilde{\mathcal{C}}(\boldsymbol{x},\omega)$, we can obtain $\tilde{\mathcal{A}}_\gamma,\tilde{\mathcal{L}}_\gamma$, and $\tilde{\mathcal{C}}_\gamma$. ∎

The error estimate of e_1 and e_2 has been proved in [15] and shown in Proposition 3.4. Now we would like to give the error estimate of e_3.

Theorem 3.6. *For the probability p defined in Lemma 3.3 and error e_3 from the random Fourier method and defined in (3.25), i.e.,*

$$e_3=\left|\left|\prod_{h=1}^{H}e^{\Delta t_h\mathcal{L}(\boldsymbol{x},\omega)}e^{\Delta t_h\mathcal{C}(\boldsymbol{x},\omega)}q-\prod_{h=1}^{H}e^{\Delta t_h\tilde{\mathcal{L}}(\boldsymbol{x},\omega)}e^{\Delta t_h\tilde{\mathcal{C}}(\boldsymbol{x},\omega)}q\right|\right|_{L^2},$$

define event

$$B_1=\left\{e_3\leq Te^{\gamma T}\left(||\boldsymbol{v}-\tilde{\boldsymbol{v}}||_{L^2}\cdot(||\nabla_{\boldsymbol{x}}q||_{L^2}+\lambda||q||_{L^2})+(\Delta t)(||\boldsymbol{v}-\tilde{\boldsymbol{v}}||_{L^2}\cdot||\nabla_{\boldsymbol{x}}q||_{L^2}+||q||_{L^2})\right)\right\}. \tag{3.30}$$

Then B_1 holds with probability greater than p, i.e., prob$(B_1)>p$.

Copyright © by SIAM and ASA. Unauthorized reproduction of this article is prohibited.

A detailed proof of Theorem 3.6 can be seen in Appendix C. Now we look back at the total error estimate in a stochastic sense. From (B.1) to (B.12), we can get the upper bounds distribution estimations of $||\boldsymbol{b}(\boldsymbol{x},\omega)||_{L^2}$,$|c(\boldsymbol{x},\omega)|$, $||\nabla_{\boldsymbol{x}} c(\boldsymbol{x},\omega)||_{L^2}$ and $||\Delta_{\boldsymbol{x}} c(\boldsymbol{x},\omega)||_{L^2}$. For any p close to 1, we can always find these four terms' corresponding upper bounds so that they are all bounded by their corresponding upper bounds with a probability greater than p. Following the selection method for γ_1 in [15], we take $\gamma_1 = \frac{2(\tilde{M}_1)^2}{\kappa} + \tilde{M}_2$ and also require γ_1 to be large enough so that $4(\frac{\gamma_1 - \tilde{M}_2}{3})^{\frac{3}{4}} \kappa^{\frac{1}{4}} > 2\kappa \tilde{M}_3 C$. Here C is defined by the fact that

$$||\nabla_{\boldsymbol{x}} q||_{L^2} \leq C ||\Delta_{\boldsymbol{x}} q||_{L^2}^{\frac{1}{2}} ||q||_{L^2}^{\frac{1}{2}}. \tag{3.31}$$

For γ_2, it should be selected large enough so that

$$||(\mathcal{L}(\boldsymbol{x},\omega) - \gamma_2) q||_{L^2} \geq \hat{C}(\kappa, \boldsymbol{b})(||\Delta_{\boldsymbol{x}} q||_{L^2} + ||q||_{L^2}); \tag{3.32}$$

here $\hat{C}(\kappa, \boldsymbol{b})$ should satisfy $\hat{C}(\kappa, \boldsymbol{b}) \geq \max(\frac{16\kappa^2 C'^2 \tilde{M}_3^2}{C_H^2}, \frac{4(\kappa \tilde{M}_4 + \tilde{M}_1 \tilde{M}_3)^2}{C_H^2})$, and C_H is the uniformly Hölder continuous coefficient. Similarly, we can select $\tilde{\gamma}_1$ and $\tilde{\gamma}_2$ according to $\tilde{\boldsymbol{b}}(\boldsymbol{x},\omega)$ and $\tilde{c}(\boldsymbol{x},\omega)$. Then we take $\tilde{\gamma} = \max(\gamma_1, \gamma_2, \tilde{\gamma}_1, \tilde{\gamma}_2)$ and $\gamma = \tilde{\gamma} + M_2^*$. Then following the proof of e_1 in [15], it can be proved that

$$e_1 \leq T e^{\gamma T} \cdot \frac{C_s}{\beta + \frac{1}{2}} (\Delta t)^{\beta - \frac{1}{2}} ||q||_{L^2}; \tag{3.33}$$

here C_s is the constant defined by the infinitesimal generator $\mathcal{A}$ and its corresponding analytical semigroup $e^{t\mathcal{A}}$ which satisfies

$$||\mathcal{A} e^{t\mathcal{A}}||_{L^2} \leq \frac{C_s}{t}, \quad t > 0. \tag{3.34}$$

Then following the proof of e_2 in [15], it can be proved that

$$e_2 \leq T e^{\gamma T} \cdot \left(\frac{4C_s}{3} (\Delta t)^{\frac{1}{2}} + (M_2^*)^2 (\Delta t) \right) ||q||_{L^2}. \tag{3.35}$$

Finally following the proof of e_3 mentioned above, we can obtain that

$$e_3 \leq T e^{\gamma T} \cdot \Big(||\boldsymbol{v} - \tilde{\boldsymbol{v}}||_{L^2} \cdot (||\nabla_{\boldsymbol{x}} q||_{L^2} + \lambda ||q||_{L^2}) + (\Delta t)(||\boldsymbol{v} - \tilde{\boldsymbol{v}}||_{L^2} \cdot ||\nabla_{\boldsymbol{x}} q||_{L^2} + ||q||_{L^2}) \Big). \tag{3.36}$$

Now we consider one realization of $\tilde{\boldsymbol{v}}(\boldsymbol{x},\omega_0) = \tilde{\boldsymbol{v}}_0(\boldsymbol{x})$ with an initial Fourier mode number N_0 and frequency step Δk. Then we can construct a sequence $\{\boldsymbol{v}_j(\boldsymbol{x})\}_{j=0}^{\infty}$ that each time we double the Fourier mode number, i.e., for $\boldsymbol{v}_j$, will have a Fourier mode number $N_j = 2^j N_0$. During the construction process of each term in one realization, we keep the values of the random variables at the previously existing truncation points unchanged and add a subdivision based on them. Due to the exponential decay performance of $E(k)$, the amplitude of the high-frequency term will exponentially decay to zero. Then we treat $\boldsymbol{v}(\boldsymbol{x}) = \lim_{j \to \infty} \boldsymbol{v}_j(\boldsymbol{x})$ as the corresponding realization of real random velocity field $\boldsymbol{v}(\boldsymbol{x})$. Now we look back to the error estimate of the correlation function of these series. From the analysis for (3.7),

Downloaded 05/24/25 to 128.195.71.97 . Redistribution subject to SIAM license or copyright; see https://epubs.siam.org/terms-privacy

Copyright © by SIAM and ASA. Unauthorized reproduction of this article is prohibited.

we know that the error of correlation function e_R is $O((N_j)^{-2})$ in this case. Due to the construction strategy mentioned, $N_j = 2^j N_0$, and then the estimate of e_R will become $O(2^{-2j})$. From this, among several different realizations, we can further give the following estimate for $\mathbb{E}_\omega[||\boldsymbol{v}(\boldsymbol{x},\omega) - \boldsymbol{v}_j(\boldsymbol{x},\omega)||_{L^2}]$:

$$\begin{aligned}(3.37)\qquad &\mathbb{E}_\omega[||\boldsymbol{v}(\boldsymbol{x},\omega) - \boldsymbol{v}_j(\boldsymbol{x},\omega)||_{L^2}^2] \\ &= \mathbb{E}_\omega\left[\int_{\mathcal{D}} |\boldsymbol{v}(\boldsymbol{x},\omega) - \boldsymbol{v}_j(\boldsymbol{x},\omega)|^2 d\boldsymbol{x}\right] \\ &= \int_{\mathcal{D}} (\mathbb{E}_\omega[\boldsymbol{v}(\boldsymbol{x},\omega)^2] - \mathbb{E}_\omega[\boldsymbol{v}_j(\boldsymbol{x},\omega)^2] - 2\mathbb{E}_\omega[(\boldsymbol{v}(\boldsymbol{x},\omega) - \boldsymbol{v}_j(\boldsymbol{x},\omega)) \cdot \boldsymbol{v}_j(\boldsymbol{x},\omega)])d\boldsymbol{x} \\ &\le \left|\int_{\mathcal{D}} R(0) - \tilde{R}_j(0) - 2\mathbb{E}_\omega[(\boldsymbol{v}(\boldsymbol{x},\omega) - \boldsymbol{v}_j(\boldsymbol{x},\omega)) \cdot \boldsymbol{v}_j(\boldsymbol{x},\omega)]d\boldsymbol{x}\right|,\end{aligned}$$

where $\tilde{R}_j(\cdot)$ is the correlation function of the generated velocity field $\boldsymbol{v}_j$. We define $\boldsymbol{v}_{res}^{(j)} = \boldsymbol{v} - \boldsymbol{v}_j$ and interpret $\boldsymbol{v}_{res}^{(j)}$ as $\boldsymbol{v}$, subtracting its components at the selected Fourier modes, and the components at other Fourier modes will still form a mean zero random field which is independent of $\boldsymbol{v}_j$. Since $\mathcal{D}$ is a bounded domain, we use S to denote its area and obtain that

$$(3.38)\qquad \mathbb{E}_\omega[||\boldsymbol{v}(\boldsymbol{x},\omega) - \boldsymbol{v}_j(\boldsymbol{x},\omega)||_{L^2}^2] \le S \cdot |R(0) - \tilde{R}_j(0)| = S \cdot e_{R,j},$$

where $e_{R,j} \overset{\text{def}}{=} |R(0) - \tilde{R}_j(0)|$ is the error between two velocity fields' corresponding correlation functions. Then we can further know that $\mathbb{E}_\omega[||\boldsymbol{v}(\boldsymbol{x},\omega) - \boldsymbol{v}_j(\boldsymbol{x},\omega)||_{L^2}^2]$ will have a convergence rate $O(2^{-2j})$. It also means that $\mathbb{E}_\omega[||\boldsymbol{v}(\boldsymbol{x},\omega) - \boldsymbol{v}_j(\boldsymbol{x},\omega)||_{L^2}]$ will at least have a convergence rate $O(2^{-j}) = O((N_j)^{-1})$, and its variance $Var(||\boldsymbol{v}(\boldsymbol{x},\omega) - \boldsymbol{v}_j(\boldsymbol{x},\omega)||_{L^2})$ will also converge to zero with a convergence rate at least $O(2^{-2j}) = O((N_j)^{-2})$. In the above analysis, we did not make further requirements on realization, and thus this convergence rate is available for arbitrary realizations. By following the perturbation theory in [10], we can obtain the following theorem.

Theorem 3.7. *In each realization, the corresponding velocity fields* $\{\boldsymbol{v}_j\}_{j=0}^{\infty}$ *and* $\boldsymbol{v}$ *will define their corresponding operators* $\{e^{\Delta t\mathcal{L}_\gamma^j(\boldsymbol{x})}e^{\Delta t\mathcal{C}_\gamma^j(\boldsymbol{x})}\}_{j=0}^{\infty}$ *and* $e^{\Delta t\mathcal{L}_\gamma(\boldsymbol{x})}e^{\Delta t\mathcal{C}_\gamma(\boldsymbol{x})}$*, and then for sufficiently large* j*,*

$$e^{\Delta t\mathcal{L}_\gamma^j(\boldsymbol{x})}e^{\Delta t\mathcal{C}_\gamma^j(\boldsymbol{x})} \to e^{\Delta t\mathcal{L}_\gamma(\boldsymbol{x})}e^{\Delta t\mathcal{C}_\gamma(\boldsymbol{x})} \text{ in the generalized sense.}$$

Also for sufficiently large j*, the principal eigenvalues of* $e^{\Delta t\mathcal{L}_\gamma^j(\boldsymbol{x})}e^{\Delta t\mathcal{C}_\gamma^j(\boldsymbol{x})}$ *and* $e^{\Delta t\mathcal{L}_\gamma(\boldsymbol{x})}e^{\Delta t\mathcal{C}_\gamma(\boldsymbol{x})}$ *are close, and their difference is small in the sense of Proposition* A.1.

Proof. Here we define $\mathcal{I}(j) = e^{\Delta t\mathcal{L}_\gamma^j(\boldsymbol{x})}e^{\Delta t\mathcal{C}_\gamma^j(\boldsymbol{x})} - e^{\Delta t\mathcal{L}_\gamma(\boldsymbol{x})}e^{\Delta t\mathcal{C}_\gamma(\boldsymbol{x})}$. Then, following (C.7) we can obtain

$$(3.39)\quad ||\mathcal{I}(j)q||_{L^2} \le (\lambda\Delta t||\boldsymbol{v} - \boldsymbol{v}_j||_{L^2} + O((\Delta t)^2))||q||_{L^2} + (\Delta t + (\Delta t)^2) \cdot ||\boldsymbol{v} - \boldsymbol{v}_j||_{L^2}||\nabla_{\boldsymbol{x}} q||_{L^2},$$

and here the term $O((\Delta t)^2)$ actually should be infinitely termed sums which all consist of the coefficient $||\boldsymbol{v} - \boldsymbol{v}_j||_{L^2}$. Due to this, we do not care so much about the term with a high Δt order, and here we still write $O((\Delta t)^2)$, but we know this term converges to zero as j

Copyright © by SIAM and ASA. Unauthorized reproduction of this article is prohibited.

Downloaded 05/24/25 to 128.195.71.97 . Redistribution subject to SIAM license or copyright; see https://epubs.siam.org/terms-privacy

goes to infinity. Then $||\nabla_{\boldsymbol{x}} q||_{L^2}$ is bounded by $||(\mathcal{A}-\gamma)q||_{L^2}$, and then we can get that it is also bounded by $C_J||e^{\Delta t\mathcal{L}_\gamma(\boldsymbol{x})}e^{\Delta t\mathcal{C}_\gamma(\boldsymbol{x})}q||_{L^2}$. Then we can obtain that $\mathcal{I}(j), j=0,1,2,\ldots$ is $e^{\Delta t\mathcal{L}_\gamma(\boldsymbol{x})}e^{\Delta t\mathcal{C}_\gamma(\boldsymbol{x})}$-bounded, and the coefficients of both the $||q||_{L^2}$ term and the $||\nabla_{\boldsymbol{x}} q||_{L^2}$ term converge to zero as j goes to infinity. Following Proposition A.4, we can get that $e^{\Delta t\mathcal{L}_\gamma^j(\boldsymbol{x})}e^{\Delta t\mathcal{C}_\gamma^j(\boldsymbol{x})} \to e^{\Delta t\mathcal{L}_\gamma(\boldsymbol{x})}e^{\Delta t\mathcal{C}_\gamma(\boldsymbol{x})}$ in the generalized sense.

Then following the spectral gap assumption and Propositions A.1 and A.5, we can obtain the fact that when adding a small perturbation $\mathcal{I}(j)$ on the original operator $e^{\Delta t\mathcal{L}_\gamma(\boldsymbol{x})}e^{\Delta t\mathcal{C}_\gamma(\boldsymbol{x})}$, the change of the principal eigenvalue is also small in the sense that the principal eigenvalue is continuous at the coefficient of the perturbation equal to zero. Then we finish the proof and can extend this conclusion to the one iteration from 0 to T. ∎

Theorem 3.8. *For sufficiently small Δt and large j, we denote the following error estimate of the random Fourier method to approximate the operator obtained by the Lie–Trotter operator splitting method (3.14) as event B_2:*

$$B_2 = \left\{ \left|\left| \prod_{h=1}^{H} e^{\Delta t\mathcal{L}}e^{\Delta t\mathcal{C}} - \prod_{h=1}^{H} e^{\Delta t\mathcal{L}_j}e^{\Delta t\mathcal{C}_j} \right|\right|_{L^2} \le C_3(\lambda,p)\sqrt{||\boldsymbol{v}-\boldsymbol{v}_j||_{L^2}^2 + (\Delta t)^2} \right\}, \tag{3.40}$$

and B_2 holds with a probability greater than p, i.e., $prob(B_2) > p$. Here p is a probability which approaches 1 (see Lemma 3.3) and to simplify notation, we use $\mathcal{L},\mathcal{C},\mathcal{L}_j,\mathcal{C}_j$ to denote $\mathcal{L}(\boldsymbol{x},\omega)$, $\mathcal{C}(\boldsymbol{x},\omega)$,$\mathcal{L}_j(\boldsymbol{x},\omega)$, $\mathcal{C}_j(\boldsymbol{x},\omega)$.

A detailed proof of Theorem 3.8 can be seen inAppendix D. Together with Proposition 3.4, Lemma 3.3 and Theorem 3.6 mentioned above, we can give an error estimate for the principal eigenvalue.

Theorem 3.9. *Let $e^{\mu(\lambda)T}$ and $e^{\mu_{\Delta t}(\lambda)T}$ denote the principal eigenvalue of the solution operator $\mathcal{U}(T,0)$ and the approximated solution operator $\prod_{h=1}^{H} e^{\Delta t_h\tilde{\mathcal{L}}(\boldsymbol{x},\omega)}\ e^{\Delta t_h\tilde{\mathcal{C}}(\boldsymbol{x},\omega)}$, respectively. For given $E(k)$ satisfying properties P1–P4, denote the following error estimate as event B_3:*

$$B_3 = \left\{ |e^{\mu(\lambda)T} - e^{\mu_{\Delta t}(\lambda)T}| \le C_4(p)\cdot(\Delta t)^{\frac{1}{2}} + C_5(\lambda,p)\cdot||\boldsymbol{v}-\tilde{\boldsymbol{v}}||_{L^2} \right\}. \tag{3.41}$$

Then B_3 holds with a probability greater than p for sufficiently small Δt and large N_F. Here p is a probability which approaches 1 (see Lemma 3.3). $\mathbb{E}_\omega[||\boldsymbol{v}-\tilde{\boldsymbol{v}}||_{L^2}]$ has a convergence rate $O((N_F)^{-1})$, and $Var(||\boldsymbol{v}-\tilde{\boldsymbol{v}}||_{L^2})$ has a convergence rate $O((N_F)^{-2})$. Moreover, we can obtain that in this case, $|\mu(\lambda)-\mu_{\Delta t}(\lambda)| = O(C_4(p)(\Delta t)^{\frac{1}{2}} + C_5(\lambda,p)\ ||\boldsymbol{v}-\tilde{\boldsymbol{v}}||_{L^2})$. To simplify notation, we denote $C_4 = C_4(p)$, $C_5 = C_5(\lambda,p)$, and

$$\mu_{IPM}(\lambda) = \lim_{N\to\infty} \frac{\sum_{h=0}^{H-1} \log\left(N^{-1}\sum_{l=1}^{N}\exp(\tilde{c}(\tilde{\xi}_h^{l,M-1})\Delta t)\right)}{H\Delta t}.$$

Combining these with the error estimate of the Lagrangian (particle) method in section 3.3, we have the following convergence result: Define event

$$B_4 = \left\{ \mu_{IPM}(\lambda) = \mu(\lambda) + O\left(\left(1-\frac{\theta}{\vartheta}\right)^M\right) + O(C_4(\Delta t)^{\frac{1}{2}}) + O(C_5||\boldsymbol{v}-\tilde{\boldsymbol{v}}||_{L^2}) \right\}. \tag{3.42}$$

Then B_4 holds with probability greater than p.

Downloaded 05/24/25 to 128.195.71.97 . Redistribution subject to SIAM license or copyright; see https://epubs.siam.org/terms-privacy

Copyright © by SIAM and ASA. Unauthorized reproduction of this article is prohibited.

Proof. According to the standard spectral theorem in [10], the principal eigenvalue of these two operators $\mathcal{U}(T,0)$ and $\prod_{h=1}^{H} e^{\Delta t_h \tilde{\mathcal{L}}(\boldsymbol{x},\omega)} e^{\Delta t_h \tilde{\mathcal{C}}(\boldsymbol{x},\omega)}$ will satisfy

$$|\mu(\lambda) - \mu_{\Delta t}(\lambda)| \leq C_{sp} \left\| \mathcal{U}(T,0) - \prod_{h=1}^{H} e^{\Delta t_h \tilde{\mathcal{L}}(\boldsymbol{x},\omega)} e^{\Delta t_h \tilde{\mathcal{C}}(\boldsymbol{x},\omega)} \right\|_{L^2}. \tag{3.43}$$

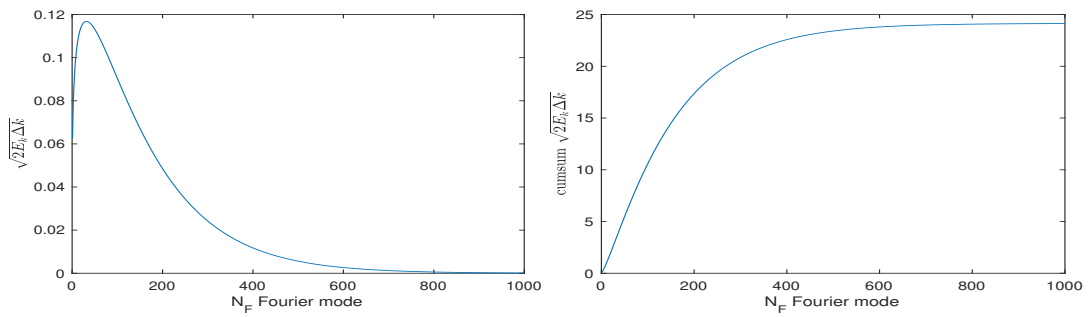
Here we first define $C_4(p) = \frac{8}{3} C_s T e^{\gamma T}$ and $C_5(\lambda, p) = 4(C_D(p) + \lambda) T e^{\gamma(T+1)}$. Follow the error estimate we analyed for $e_1, e_2, e_3, ||\boldsymbol{v} - \tilde{\boldsymbol{v}}||_{L^2}$, and Theorem 3.8. By the triangle inequality, we can get (3.41). Then we can accordingly obtain the error estimate for $|\mu(\lambda) - \mu_{\Delta t}(\lambda)|$. Thus due to the analysis in section 3.3 and by triangle inequality, we get the convergence result (3.42). ∎

4. Numerical experiments. We present several numerical examples computed by the IPM. We first show examples to verify the convergence and accuracy of the IPM method in computing μ. Then we consider 2D and 3D random fields with the equispaced discrete spectrum where $\Delta k = \frac{1}{20\pi}$ and compute front speeds c^* of these cases. Meanwhile, we investigate and analyze the relationship between c^* and the magnitude of the velocity fields on torus $\mathcal{D}$. We take domain size to infinity and study the finite domain effect of c^* on $\mathbb{R}^d$ by a normalized/centered IPM. Such an unbounded domain problem is impossible to compute by mesh-based methods without a proper domain truncation.

4.1. Convergence test in computing μ. The convergence test of the operator splitting method and using the IPM method in computing principal eigenvalues of determined flows can be seen in [15]. In contrast to the test in the deterministic velocity field, here we also need to verify the convergence between generated random fields (using the random Fourier method [16]) and real random potential fields. Here we choose a specific $E(k)$ which satisfies properties P1 –P4 proposed in section 3.1,

$$E(k) = |k|^{\frac{1}{2}} e^{-|k|}. \tag{4.1}$$

We plot the performance of the coefficient of the generated random velocity field. From Figure 1 we see that as frequency k goes to infinity, the coefficient of the corresponding Fourier



(a) Coefficient value of Fourier mode (b) Cumsum of coefficient value

Figure 1. *Performance of the coefficient of the generated random velocity field.*

Downloaded 05/24/25 to 128.195.71.97 . Redistribution subject to SIAM license or copyright; see https://epubs.siam.org/terms-privacy

Copyright © by SIAM and ASA. Unauthorized reproduction of this article is prohibited.

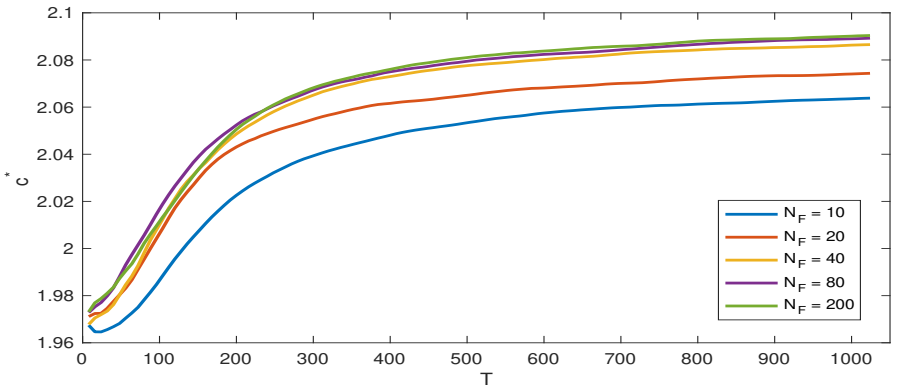


Figure 2. *Front speed c^* vs. t of random shear flow with different Fourier modes N_F.*

mode term in the generated random velocity field goes to 0. We also test convergence using the random Fourier method generated velocity in computing the principal eigenvalues for a 2D random shear flow $v(x,y) = \delta \cdot (0, \xi(x))$. Here $\delta = \frac{1}{40}$, and $\xi(x)$ is set as follows:

$$\xi(x) = \sum_{j=0}^{N_F} \sqrt{2E(k_j)\Delta k_j} \cdot [\zeta_j \cos(2\pi k_j x) + \eta_j \sin(2\pi k_j x)]. \tag{4.2}$$

We can see from Figure 2 that in one random realization, as we increase the Fourier modes number, the principal eigenvalues we get are very close when the Fourier modes number N_F is near or larger than 200 in this case.

4.2. IPM vs. semi-Lagrangian computation of KPP front speed.

4.2.1. 2D cellular flow. We compare the interacting particle method and the spectral and semi-Lagrangian methods in computing KPP front speeds in 2D cellular flow:

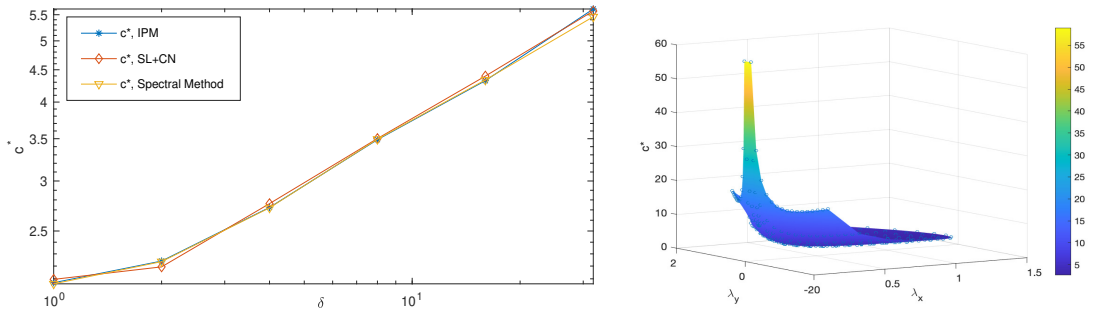
$$v(x,y) = \delta \cdot (-\sin(x)\cos(y),\ \cos(x)\sin(y)). \tag{4.3}$$

We take the spectral method as a benchmark and select δ from 2^0 to 2^4. Figure 3a shows that these three methods give similar results. The log-log fitted curve has a slope of 0.257 so that $c^* = O(\delta^{0.257}) \approx O(\delta^{0.25})$, consistent with theory [26]. In Figure 3a, the semi-Lagrangian and spectral methods are in agreement. Figure 3b is an example of searching $\lambda \boldsymbol{e}$ to reach minimal front speed. Here $\boldsymbol{z} = (1,0)$. We do a grid search for the optimal vector $\lambda \boldsymbol{e}$ and determine $c^*(\boldsymbol{z})$ by its variational formula. We found that the optimal dual direction vector $\boldsymbol{e}$ is either equal to $\boldsymbol{z}$ or near $\boldsymbol{z}$. The former occurs for random flows and reduces the search to only the scalar variable λ, thereby saving computation time. The latter occurs for flows with ordered streamlines (e.g., cellular flows) for which a local search around $\boldsymbol{z}$ suffices instead of a time-consuming global research.

4.2.2. 2D random shear flow. Now we adjust the velocity field with only the generated random shear field, i.e., $v(x,y) = \delta \cdot (0, \xi(x))$. Here we would like to simulate the case in $\mathbb{R}^2$. We can see that given sufficient Monte Carlo number N and evolution time n in the

Downloaded 05/24/25 to 128.195.71.97 . Redistribution subject to SIAM license or copyright; see https://epubs.siam.org/terms-privacy

Copyright © by SIAM and ASA. Unauthorized reproduction of this article is prohibited.



(a) Comparison of c^* in 2D cellular flow

(b) Search for $\lambda \boldsymbol{e}$, $\delta = 2^2$

Figure 3. *Computation of c^* in 2D cellular flow.*

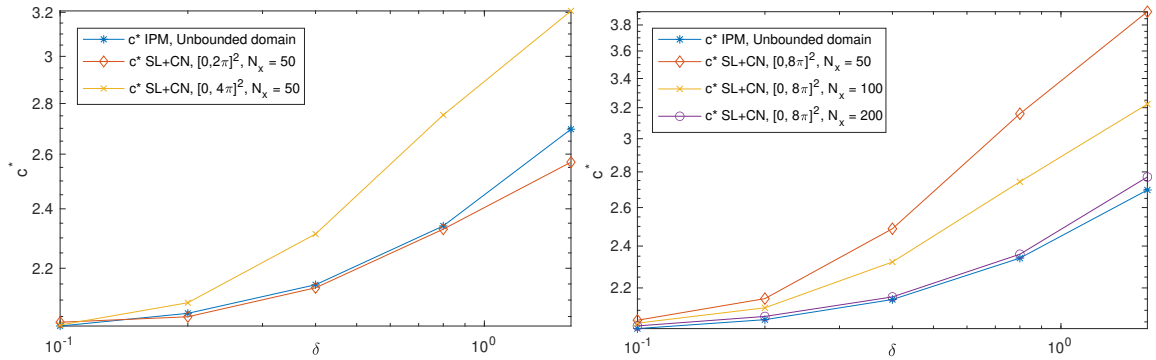
IPM, the semi-Lagrangian method needs increasingly fine grids to get similar results. And during the process where we enlarge the domain to "infinity," for the IPM, we just need to change the initial distribution and similarly compute the particle traces. This does not have any effect on the computation time. For the semi-Lagrangian method, as we enlarge the domain, we will need to increase the number of grids if we want to maintain the same partition accuracy. We compute the KPP front speed c^* in different domain settings by these two methods with the same random realization. As in [24], for the advection-reaction step, we use a semi-Lagrangian scheme, and for the diffusion step, we use an implicit Crank–Nicolson scheme in time and spectral method in space. We denote this method as SL + CN. In the SL + CN method, if we would like to simulate the situation with an unbounded domain, we can only enlarge the domain step by step. For example, we start with the domain $[0, 2\pi]^2$ and enlarge it to $[0, 4\pi]^2$, $[0, 8\pi]^2$, ... In the Eulerian framework of the SL + CN method, we need to divide the whole domain into $N_x \times N_y$ grids. Here for simplicity, we just assume $N_x = N_y$, and if we want to maintain the mesh size during the process of enlarging the domain, the time cost will get more and more expensive. If we would like to maintain the time cost, then the accuracy of the SL + CN method will get worse and worse. The time complexity of the semi-Lagrangian method is proportional to the number of grid points; i.e., if we set domain length as L and maintain the mesh size, then the advection-reaction step's time complexity is $O(N_x^2) = O(L^2)$ in 2D cases. Benefiting from the FFT algorithm, the time complexity of the diffusion step is $O(L \log L)$. Time cost will become more expensive when we consider 3D cases by SL + CN.

It is seen from Figures 4a and 4b that as the domain size L gets larger, more grid points are needed to maintain the accuracy of the SL + CN method.

4.3. 3D cases' time complexity. Meanwhile, we also test the time cost of the SL + CN method in 3D cellular flow with evolution time $T = 100$ and varying meshgrid sizes. For the meshgrids $30 \times 30 \times 30$, $35 \times 35 \times 35$, and $40 \times 40 \times 40$, since it takes too long to evolve, and the computational cost of each step of the evolution is similar, we only evolve one-tenth of the whole process, i.e., $T = 10$, and estimate the computation time of the whole evolution process, i.e., $T = 100$. As illustrated in Figure 5, the computational time complexity is $O((N_x)^{7.90}) \approx O((N_x)^8)$. This is due to the fact that the time complexity of an implicit format solver implemented using sparse matrices will be between $O((N_x)^6)$ and $O((N_x)^9)$

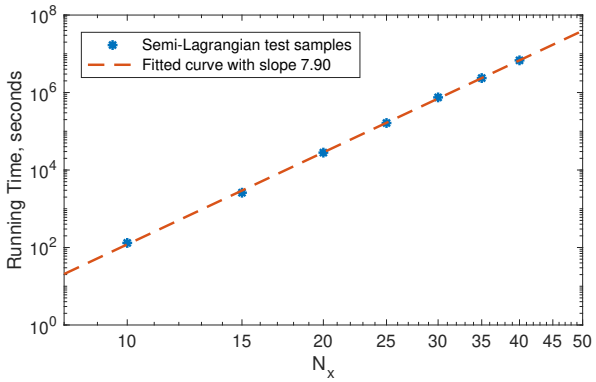
Copyright © by SIAM and ASA. Unauthorized reproduction of this article is prohibited.

Downloaded 05/24/25 to 128.195.71.97 . Redistribution subject to SIAM license or copyright; see https://epubs.siam.org/terms-privacy



(a) Same N_x, different domain lengths (b) Same domain length, different N_x

Figure 4. *Comparison of c^* by IPM and SL + CN method.*



Mesh size	Running time
$10 \times 10 \times 10$	1.31×10^2s
$15 \times 15 \times 15$	2.58×10^3s
$20 \times 20 \times 20$	2.81×10^4s
$25 \times 25 \times 25$	1.63×10^5s
$30 \times 30 \times 30$	7.49×10^5s *
$35 \times 35 \times 35$	2.36×10^6s *
$40 \times 40 \times 40$	6.77×10^6s *

Figure 5. *Log-log plot and table of mesh size N_x vs. running time of SL + CN method in 3D cellular flow (* in the table means the time is estimated).*

depending on the characteristics and structure of the sparse matrices. Such a time complexity is undoubtedly hard to accept when the SL + CN method would like to reach high resolution, and the memory cost is also substantial. If we use the explicit scheme, such as the Runge–Kutta 2 (RK2) scheme, since the entire format is implemented using sparse matrices, the time complexity illustrated in Figure 6 is $O((N_x)^{2.90}) \approx O((N_x)^3)$. Due to the CFL condition and other constraints, we have to shrink the time step Δt when we increase the number of meshgrid points N_x. With adaptive time step Δt, the SL + RK2 method's time complexity shown in Figure 6 is $O((N_x)^{4.90}) \approx O((N_x)^5)$. We take the calculation with the mesh size of $80 \times 80 \times 80$ as a reference. To achieve the reference result of 0.01 tolerance, the SL + RK2 method requires 1.26×10^4 seconds, while our IPM takes only 7.62×10^2 seconds.

4.4. IPM computation of KPP front speeds in random flows.

4.4.1. Random 2D cellular flow. Here we change the velocity field into 2D cellular flow with random perturbation. The approximation to the random perturbation is generated by

Downloaded 05/24/25 to 128.195.71.97 . Redistribution subject to SIAM license or copyright; see https://epubs.siam.org/terms-privacy

Copyright © by SIAM and ASA. Unauthorized reproduction of this article is prohibited.

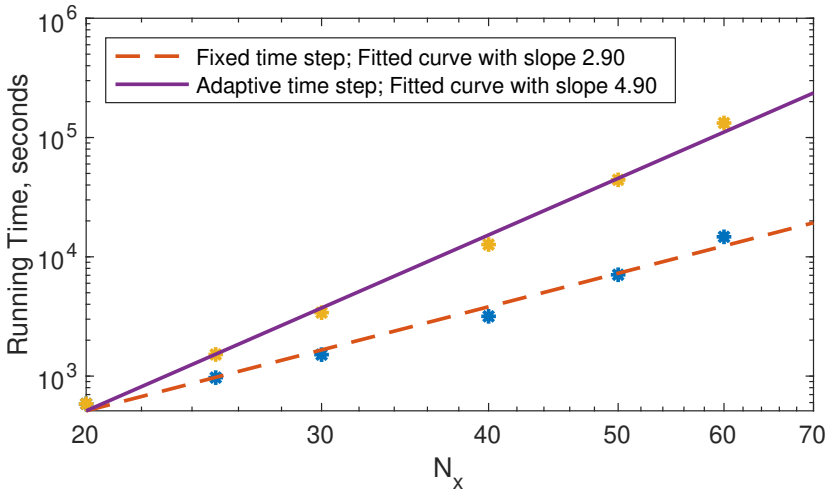


Figure 6. *Log-log plot of mesh size N_x vs. running time.*

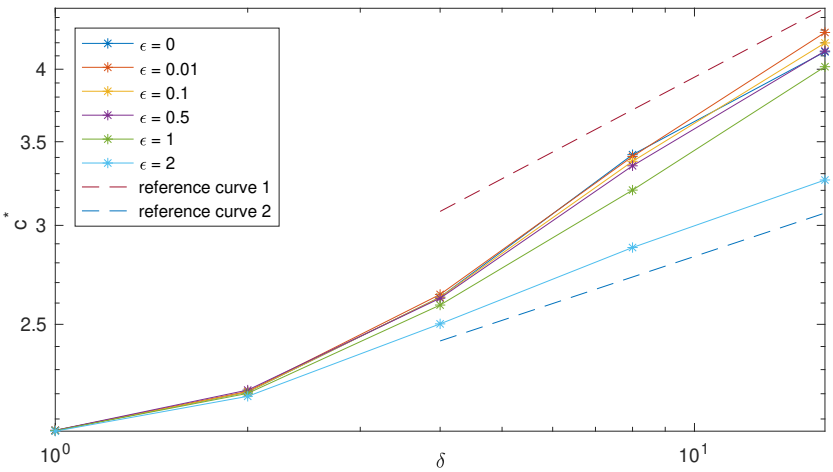


Figure 7. *Log-log plot of c^* vs. δ in 2D random cellular flow at different ϵ; $z = (1,0)$.*

the random Fourier method; i.e., $v(x,y)$ is now changed into

$$v(x,y) = \delta \cdot (-\sin(x)\cos(y),\ \cos(x)\sin(y) + \epsilon \cdot \xi(x)). \tag{4.4}$$

Here $\xi(x)$ is defined in the same way as (4.2) and follows the same energy spectral density $E(k)$ defined in (4.1). This is a 2D cellular flow with a random perturbation. In this numerical experiment, we set the iteration number $n = 256$, $\Delta t = 2^{-9}$, and Monte Carlo number $N =$ 100,000 (sufficiently large). For the random velocity field with $\Delta k = \frac{1}{20\pi}$, we set $N_F = 400$, $k_j = j\Delta k$. Then we compute the KPP front speeds with different coefficients of the random perturbation.

In Figure 7, the two reference curves are with slopes of 0.26 and 0.17. Here we compute 30 realizations and take their averages. During the computation process, we found that the

Downloaded 05/24/25 to 128.195.71.97 . Redistribution subject to SIAM license or copyright; see https://epubs.siam.org/terms-privacy

Copyright © by SIAM and ASA. Unauthorized reproduction of this article is prohibited.

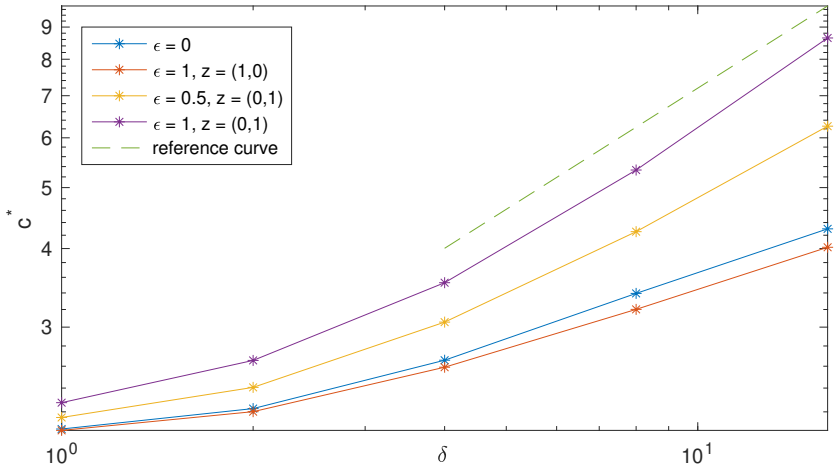


Figure 8. *Log-log plot of c^* vs. δ in 2D random cellular flow with different ϵ and z.*

variance of these different realization samples is very small. Then from Figure 7, we can see that (1) as the coefficient of the random term ϵ is not equal to zero and increases, the front speed with direction $\boldsymbol{z} = (1,0)$.This term demonstrates the power-law scaling of c^* concerning δ, and the fitted curves' slope is getting smaller and smaller; (2) as the coefficient of the random term ϵ is decreasing and converging to zero, the front speed c^* converges to the case with no random term (i.e., $\epsilon = 0$).

Then we changed the direction $\boldsymbol{z} = (0,1)$ and kept other parameters the same and got Figure 8. In Figure 8, the reference curve's slope is 0.64. We can see that if we change the direction $\boldsymbol{z}$ to $(0,1)$, then as the random coefficient ϵ increases, the front speed c^* will also increase.

Then we compare the invariant measure of 2D cellular flow with and without the addition of a random perturbation term on 2D torus $\mathcal{D}$. From Figure 9, by comparing the subfigures without random term (left: 9a and 9c) to the invariant measure of the subfigures with the random term (right: 9b and 9d), we can see that the addition of the random term creates a degree of disruption to original invariant measure.

4.4.2. 2D random shear flow. In this subsection, we changed the velocity field into the generated random shear flow, i.e.,

$$\boldsymbol{v} = v(x,y) = \delta \cdot (0,\ \xi(x)). \tag{4.5}$$

With this random shear velocity field flow setting, we consider the front speed c^* with direction $\boldsymbol{z} = (0,1)$. After searching for the direction $\boldsymbol{e}$, we found that $\boldsymbol{e} = (1,0)$ can reach the front speeds. For $\boldsymbol{e} = (1,0)$, we can analyze this case from the system

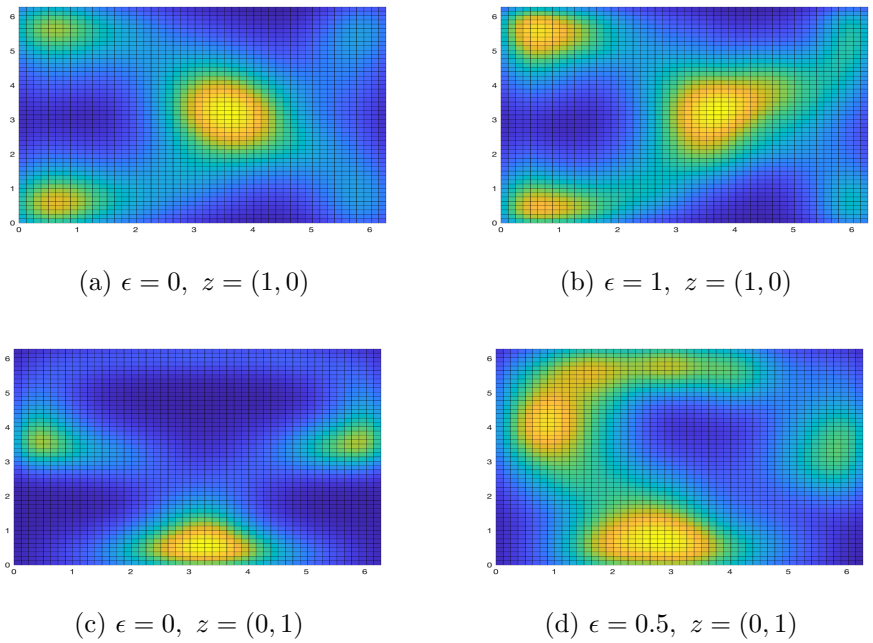
$$q_t = \mathcal{A}q \overset{\text{def}}{=} \kappa \Delta_{\boldsymbol{x}} q + (-2\kappa\lambda \boldsymbol{e} + \boldsymbol{v}) \cdot \nabla_{\boldsymbol{x}} q + (\kappa\lambda^2 - \lambda \boldsymbol{v} \cdot \boldsymbol{e} + f'(0))q. \tag{4.6}$$

Decompose the operator $\mathcal{A}$ into $\mathcal{A} = \mathcal{L} + \mathcal{C}$, where

$$\mathcal{L} = \kappa \Delta_{\boldsymbol{x}} + (-2\kappa\lambda \boldsymbol{e} + \boldsymbol{v}) \cdot \nabla_{\boldsymbol{x}} \text{ and } \mathcal{C} = (\kappa\lambda^2 - \lambda \boldsymbol{v} \cdot \boldsymbol{e} + f'(0)). \tag{4.7}$$

Copyright © by SIAM and ASA. Unauthorized reproduction of this article is prohibited.

Downloaded 05/24/25 to 128.195.71.97 . Redistribution subject to SIAM license or copyright; see https://epubs.siam.org/terms-privacy



(a) $\epsilon = 0,\ z = (1,0)$ (b) $\epsilon = 1,\ z = (1,0)$

(c) $\epsilon = 0,\ z = (0,1)$ (d) $\epsilon = 0.5,\ z = (0,1)$

Figure 9. *Comparison of invariant measure in 2D (random) cellular flow.*

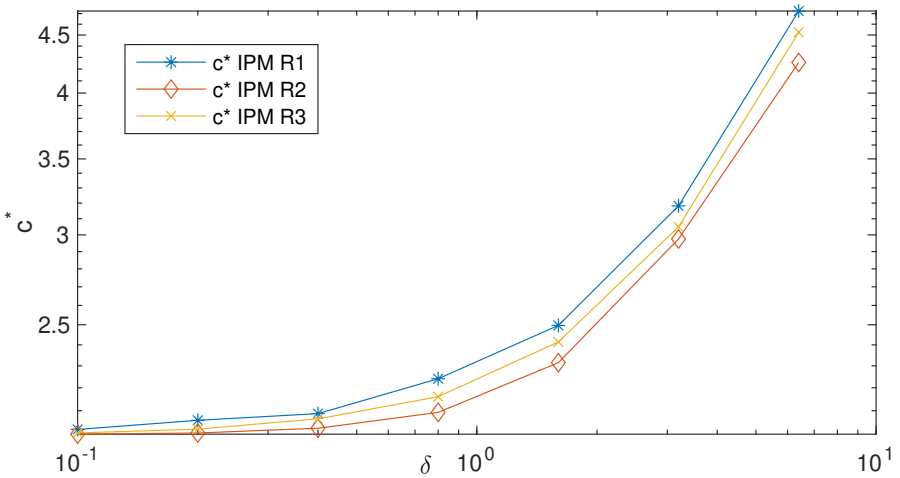


Figure 10. *Log-log plot of c^* vs. δ , $z = (0,1)$, 2D random shear flow by IPM.*

When $\boldsymbol{e} = (1,0)$, we can see that $\boldsymbol{v} \cdot \boldsymbol{e} = 0$; the potential is always a constant. Only a shift has an effect on particles and reflects the front speed c^*. So no matter how we change the amplitude of the velocity field δ, the front speed c^* will always remain at a constant.

So, here we only consider the front speed c^* with $\boldsymbol{z} = (0,1)$ in this random shear flow setting. Additionally, at this time we do not limit the domain $\mathcal{D}$ but enlarge it to infinity ($\mathbb{R}^2$). In the following experiments with an unbounded domain setting, we initialize the particles with uniform distribution on $\mathcal{D}$. Then the particles can spread among unbounded

Copyright © by SIAM and ASA. Unauthorized reproduction of this article is prohibited.

Downloaded 05/24/25 to 128.195.71.97 . Redistribution subject to SIAM license or copyright; see https://epubs.siam.org/terms-privacy

domains, and we give them sufficient time to move and spread out. By realizing the random shear velocity field with different random seeds, we compute the KPP front speeds c^*; the results are shown in Figure 10.

4.4.3. 3D random ABC flow. Here we change the velocity field into 3D ABC flow with random perturbation, i.e., the velocity field is changed into

$$v(x,y,z) = \delta \cdot (\sin(z) + \cos(y),\ \sin(x) + \cos(z) + \epsilon \cdot \xi(x),\ \sin(y) + \cos(x)). \tag{4.8}$$

Also here we set $n = 512$, $\Delta t = 2^{-11}$, $N = 100{,}000$, and $\epsilon = 0$ first. Then we compute the front speed c^* with three realizations and take their average.

From Figure 11 we can see the result that the fitted curve's slope in log scale at relatively large δ is 0.9842, i.e. $c^* = O(\delta^{0.9842}) \approx O(\delta^1)$. This means the fitted curve's slope is close to the reference curve with slope $= 1$ in log scale at relatively large δ. This result is consistent with the result in [30].

Now if we change the random coefficient ϵ to make it not equal to 0 and compute the front speed c^* corresponding to these cases, then we will find in Figure 12 that, with the addition of a random term and increasing its amplitude, c^* in 3D ABC flow will get smaller and smaller. This is because the random term gradually destroys the principal vortex structure [3] (ballistic orbits [38, 9, 18]) in the ABC flow.

4.4.4. 3D random cellular flow. Here we consider the 3D cellular flow with random perturbation; the velocity field is changed into

$$v(x,y,z) = \delta \cdot (-\sin(x)\cos(y)\cos(z),\ -\sin(y)\cos(x)\cos(z) + \epsilon \cdot \xi(x),\ 2\sin(z)\cos(x)\cos(y)). \tag{4.9}$$

Here we set $n = 512$, $\Delta t = 2^{-11}$, $N = 100{,}000$, $\epsilon = 0, 0.1, 0.4, 1, 2$ and compute their corresponding c^*.

In Figure 13, the reference curve has a slope of 0.13. We can see that when $\epsilon = 0$, the fitted curve has the slope 0.1351, and this result is consistent with the result in [30]. As the

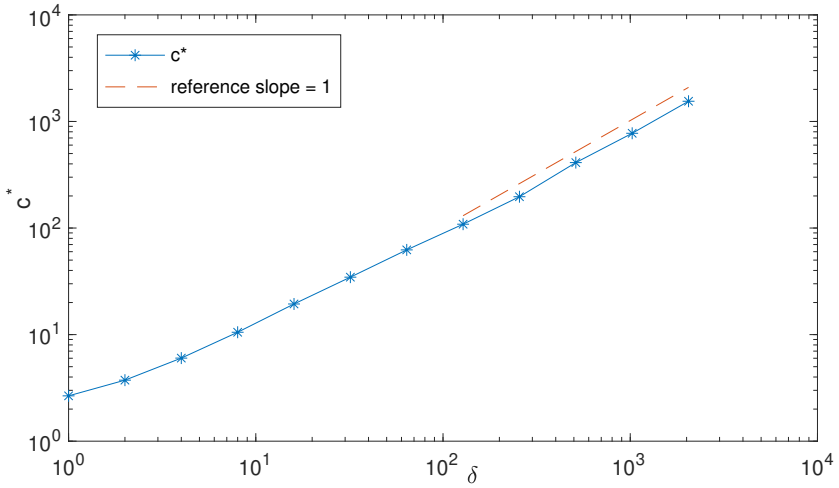


Figure 11. *Log-log plot of c^* vs. δ, $\epsilon = 0, z = (0,1,0)$, 3D ABC flow.*

Downloaded 05/24/25 to 128.195.71.97 . Redistribution subject to SIAM license or copyright; see https://epubs.siam.org/terms-privacy

Copyright © by SIAM and ASA. Unauthorized reproduction of this article is prohibited.

random perturbation strengthens by tuning up ϵ, the corresponding slopes of the fitted curves and c^* values getlarger. The addition of the random perturbation term destroys the closed streamline structures in 3D cellular flow (reduces trapping) and enhances particle transport, and thereby c^* increases.

4.5. IPM with dynamic shift for particles on $\mathbb{R}^d$. By removing the boundary restriction step in Algorithm 2.1, IPM can be readily implemented for computing c^* on $\mathbb{R}^d$. In order to investigate whether the c^* computed by IPM with gradually increasing domain sizes will converge to unbounded domain results, we conduct experiments on the randomly perturbed 2D cellular flow (4.4). Figure 14 shows that as the domain size becomes larger, the c^* computed with the same random realization converges to the direct result on the unbounded domain.

In the convergence analysis of section 3, we require a bounded domain (e.g., $\mathcal{D}$) to guarantee the existence of the principal eigenvalue and carry out the subsequent c^* error analysis.

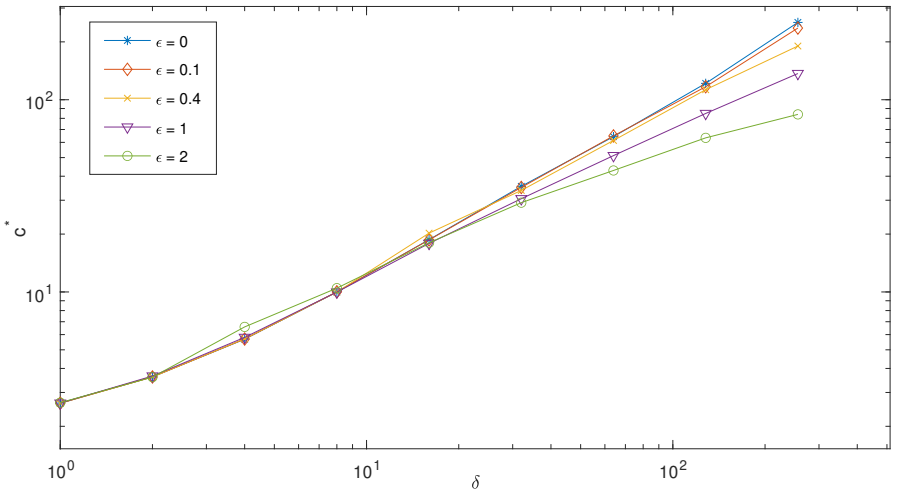


Figure 12. *Log-log plot of c^* vs. δ with different ϵ, 3D random ABC flow.*

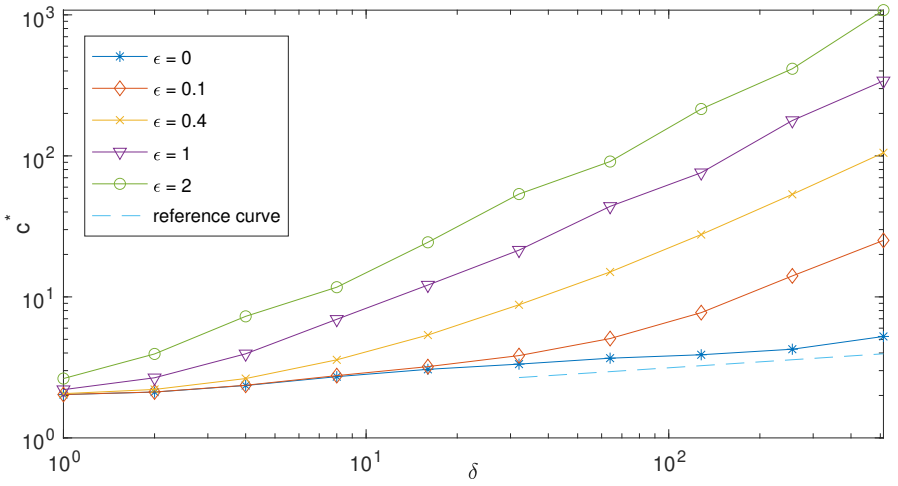


Figure 13. *Log-log plot of c^* vs. δ at different ϵ, 3D random cellular flow.*

Downloaded 05/24/25 to 128.195.71.97 . Redistribution subject to SIAM license or copyright; see https://epubs.siam.org/terms-privacy

Copyright © by SIAM and ASA. Unauthorized reproduction of this article is prohibited.

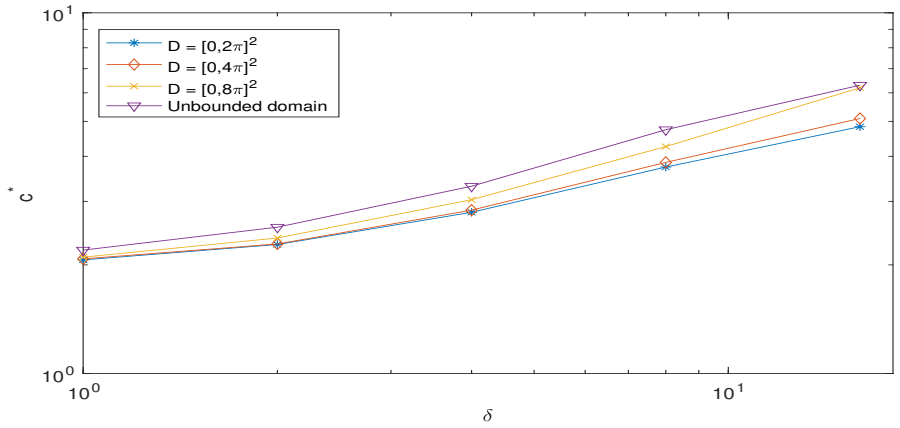


Figure 14. *Log-log plot of c^* vs. δ as domain size increases, $\epsilon = 0.5$, 2D random cellular flow.*

In a future theoretical analysis on unbounded domains, we will work with the Lyapunov exponent as a limit of principal eigenvalue in the infinite volume limit of $\mathcal{D}$ (as $\mathrm{vol}(\mathcal{D}) \uparrow \infty$) similarly to the periodization approach to stochastic homogenization [11, 7]. Our IPM can be adapted (dropping domain restriction in step 4) to compute particle distribution on unbounded domains ($\mathbb{R}^d$) directly. Different from the $\mathcal{D}$ case, the convergence to an invariant measure requires a dynamic shift to remove a mean flow-induced drift.

The SDE system (2.12), due to $\boldsymbol{b} = -2\kappa\lambda\boldsymbol{e} + \boldsymbol{v}$ and $\boldsymbol{v}$ being mean zero, has a nonzero mean drift $-2\kappa\lambda\boldsymbol{e}$. If we do not have particle motion limited on a bounded domain, the particles spread due to nonzero mean drift and do not converge to an invariant measure at large times. To make sense of convergence, we introduce a dynamic shift to center the particle ensemble over j generations (each of duration T). At each j, we shift all particles in the ensemble by $2j\kappa\lambda T$. Due to the stationarity of the random flows, the statistics of the particle evolution are invariant. After the principal eigenvalue approximations have converged, we postprocess and map the particle ensemble back to a bounded domain for visualization, for example, $\mathbb{T}^d = [0, 2\pi]^d$, then map with function $mod(\cdot)$, the multidimensional modulo operation. To summarize, the particle distribution at the output of the dynamically shifted IPM without domain restriction on $\mathbb{R}^d$ converges to an invariant measure subject to deterministic mapping.

4.5.1. 2D random shear flow.

$$\boldsymbol{v} = v(x, y) = \delta \cdot (0,\ \xi(x)). \tag{4.10}$$

We analyze IPM performance in the two cases $\boldsymbol{e} = (1, 0)$ and $\boldsymbol{e} = (0, 1)$. When $\boldsymbol{e} = (0, 1)$, $\boldsymbol{v} \cdot \boldsymbol{e} = \delta \cdot \xi(x)$, the eigenfunction only depends on x. In operator $\mathcal{L}$, $(-2\kappa\lambda\boldsymbol{e} + \boldsymbol{v}) = (0,\ \delta \cdot \xi(x) - 2\kappa\lambda)$ and $\nabla_{\boldsymbol{x}} = (\cdot, 0)$. The inner product of the two terms is zero. This operator is then a 1D random Schrödinger operator in x with well-known localization property. When $\boldsymbol{e} = (1, 0)$, $\boldsymbol{v} \cdot \boldsymbol{e} = 0$, the potential is always a constant, adding a translation on the particle. To see the effect of adding a space random perturbation term on the 2D cellular flow, we investigate how the invariant measure (particle distribution) changes after we dynamically shift the positions of particles. Here we set $\delta = 2^2$, $N = 200{,}000$, and other parameters remain the same.

Copyright © by SIAM and ASA. Unauthorized reproduction of this article is prohibited.

Downloaded 05/24/25 to 128.195.71.97 . Redistribution subject to SIAM license or copyright; see https://epubs.siam.org/terms-privacy

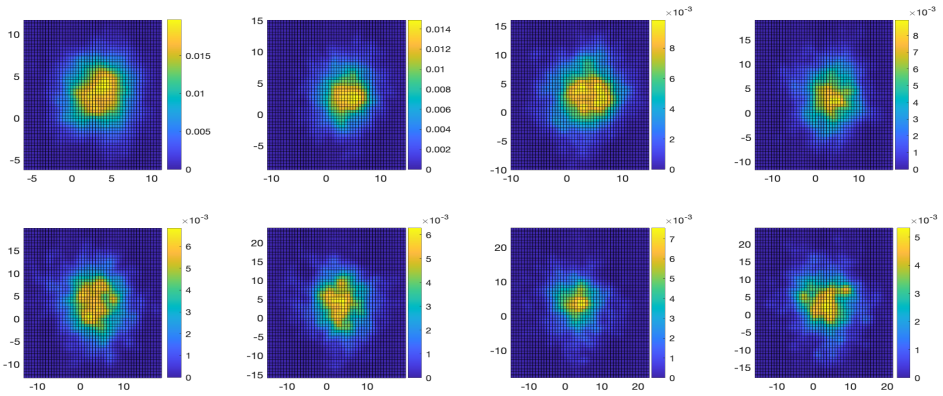
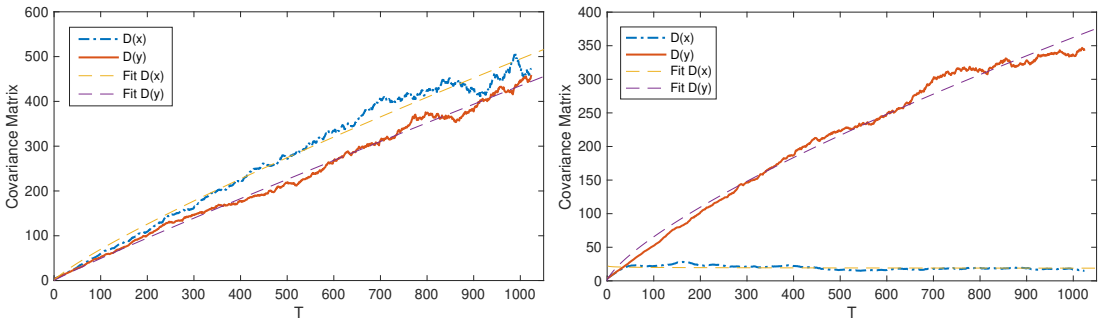


Figure 15. *Particles distribution under dynamic shift,* $t = 8$ *to* $t = 64$, $e = (1, 0)$.



(a) $\boldsymbol{e} = (1, 0)$ (b) $\boldsymbol{e} = (0, 1)$

Figure 16. *Covariance matrix evolution with different* $\mathbf{e}$, *from* $t = 0$ *to* $t = 1024$.

Here we can see from Figure 15 that, at the early stage of the experiment, the particles are continually spreading outwards from the initial area. A similar case occurs with $\boldsymbol{e} = (0, 1)$. For the performance of the particle distribution at long times, we use the rescaled center $E(\cdot)$ and the second-order momentum $D(\cdot)$ of the particles to express them. We take their average value over 10 realizations. In Figure 16a, the order of the diffusion in direction x and direction y are, respectively, $D(x) = O(t^{0.850})$ and $D(y) = O(t^{0.945})$. In Figure 16b, the order of the diffusion in direction x and direction y are, respectively, $D(x) = O(t^{-0.013}) \approx O(t^0)$ and $D(y) = O(t^{0.742})$.

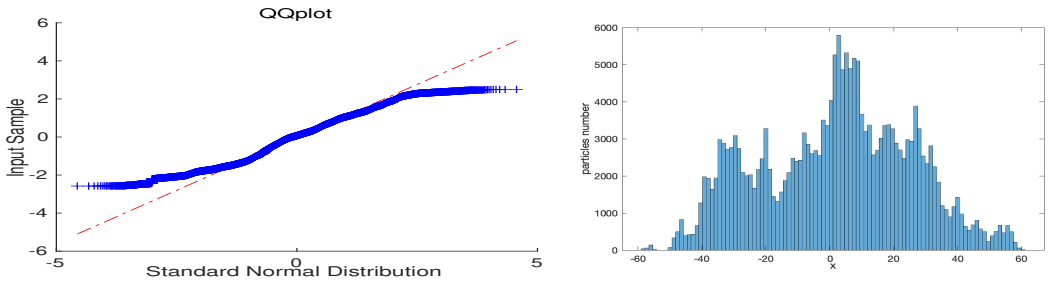
We also perform common statistical tests of the particle distribution at $t = 1024$ (e.g., QQplot and histogram in Figure 17), and the results all show that the particle distribution is non-Gaussian. In fact, according to the variation of the variance $D(x), D(y)$ with time t, it can be seen that the diffusion of the particles after the recenter process exhibits subdiffusion phenomena.

4.5.2. 3D randomly perturbed ABC flow.

$$v(x, y, z) = \delta \cdot (\sin(z) + \cos(y),\ \sin(x) + \cos(z) + \epsilon \cdot \xi(x),\ \sin(y) + \cos(x)). \tag{4.11}$$

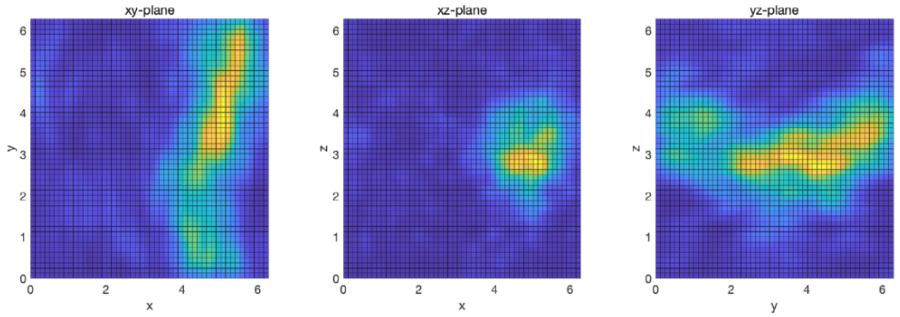
Downloaded 05/24/25 to 128.195.71.97 . Redistribution subject to SIAM license or copyright; see https://epubs.siam.org/terms-privacy

Copyright © by SIAM and ASA. Unauthorized reproduction of this article is prohibited.

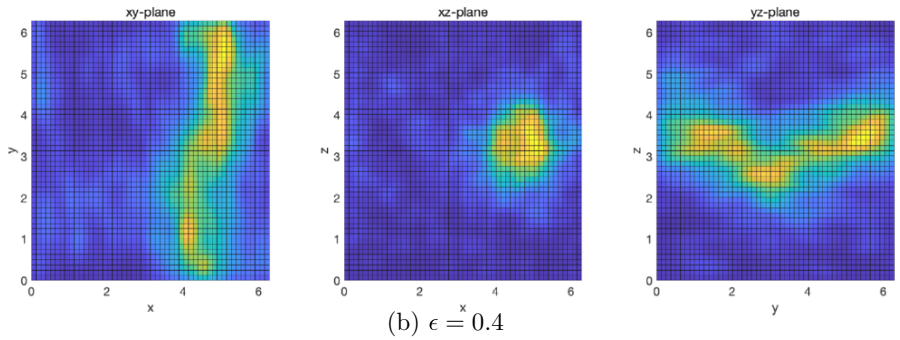


(a) QQ plot in x, $\boldsymbol{e} = (1, 0)$ (b) histogram in x, $\boldsymbol{e} = (1, 0)$

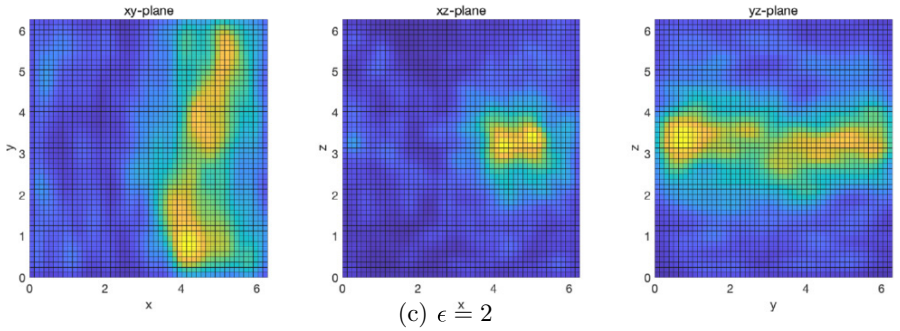
Figure 17. *QQ plot and histogram plot for random shear flow,* $\boldsymbol{e} = (1, 0), t = 1024$.



(a) $\epsilon = 0$



(b) $\epsilon = 0.4$



(c) $\epsilon = 2$

Figure 18. *Three planar views of particle distributions for randomly perturbed ABC flow at* $\epsilon = 0, 0.4, 2$, *showing increased blurring/broadening effect of perturbations.*

Downloaded 05/24/25 to 128.195.71.97 . Redistribution subject to SIAM license or copyright; see https://epubs.siam.org/terms-privacy

Copyright © by SIAM and ASA. Unauthorized reproduction of this article is prohibited.

Downloaded 05/24/25 to 128.195.71.97 . Redistribution subject to SIAM license or copyright; see https://epubs.siam.org/terms-privacy

Here we plot the distribution of the particles with different random coefficients in $\mathbb{T}^3$. It can be seen from Figure 18, especially in the xz-plane, that as the coefficient of the random term gradually increases, the radius of the exhibited tube structure becomes larger and larger with the same total number of particles, which means that the distribution of particles becomes more and more dispersed, and the tube structure is more and more severely damaged. A similar case also occurs if we change the system with an unbounded domain setting and at the final plot step restrict the distribution of the particles on $\mathbb{T}^3$.

5. Conclusions. In this paper, we developed an efficient IPM to compute KPP front speeds c^* in 2D and 3D stochastic flows, with convergence analysis based on the random Fourier method. We first computed c^* in periodic flows, including 2D cellular flow and 3D ABC flow, to reach agreement with semi-Lagrangian and spectral methods. Then we computed and analyzed the effect of random perturbations on c^*. As the perturbation strengths increased, we observed that the vortical structures (ballistic orbits) [3, 38, 18, 9] in 3D ABC flow are collapsing, resulting in smaller c^*. Compared with mesh-based methods, IPM has the following striking advantages: (1) It is scalable in spatial dimension and can easily handle stochastic 3D problems; (2) it is scalable in domain size and can handle infinite domain as well as Lyapunov exponent approximation directly. In experiments on $\mathbb{R}^3$, the empirical particle distributions from IPM show convergence under dynamic normalization, while the average particle fitness approximates the Lyapunov exponent.

Appendix A. Convergence of perturbed μ. We review the perturbation theory of linear operators with the following notation:

$$T(a) = T + a \cdot T'. \tag{A.1}$$

Here T is the original operator, T' is the perturbation operator, and a is the coefficient of the perturbation term. Then we have the following property.

Proposition A.1. *Let $T(a)$ be continuous at $a = 0$; then the eigenvalues of $T(a)$ are continuous at $a = 0$. If λ is an eigenvalue of $T(0) = T$, then the λ-group is well-defined for sufficiently small $|a|$, and the total projection $P(a)$ for the λ-group is continuous at $a = 0$.*

Next, we would like to introduce some notation to describe the convergence between operators in the generalized sense.

Definition A.2. *Consider closed linear manifolds M and N of a Banach space Z. We use S_M to denote the unit sphere of M (the set of all $v \in M$ which satisfy $||v|| = 1$). For any two closed linear manifolds M, N of Z, we define*

$$\delta(M, N) = \sup_{u \in S_M} dist(u, M), \tag{A.2}$$

$$\tilde{\delta}(M, N) = \max[\delta(M, N), \delta(N, M)]^1. \tag{A.3}$$

Definition A.3. *We denote that T_n converge to T in the generalized sense if $\tilde{\delta}(T_n, T) \to 0$.*

The following proposition that is a sufficient condition for the generalized convergence, and its proof can be found in [10].

Copyright © by SIAM and ASA. Unauthorized reproduction of this article is prohibited.

Downloaded 05/24/25 to 128.195.71.97 . Redistribution subject to SIAM license or copyright; see https://epubs.siam.org/terms-privacy

Proposition A.4. *Let $T \in \mathcal{C}(X,Y)$. Let $A_n, n = 0,1,2,\ldots,$ be T-bounded so that $||A_n v|| \le a_n||v|| + b_n||Tv||$ for $v \in D(T) \subset D(A_n)$. If $a_n \to 0$ and $b_n \to 0$, then $T_n = T + A_n \in \mathcal{C}(X,Y)$ for sufficiently large n and $T_n \to T$ in the generalized sense.*

Next, we would like to review some results which can make the above propositions applicable to an infinite system. Here we use $\Sigma(T)$ to denote the spectrum of the operator $T \in \mathcal{C}(X)$, and we suppose that the spectrum $\Sigma(T)$ has an isolated point λ. Then obviously we can divide $\Sigma(T)$ into two parts $\Sigma'(T)$ and $\Sigma''(T)$. Here $\Sigma'(T)$ consists of the single point λ and any simple closed curve Γ enclosing λ, but no other point in $\Sigma(T)$ may be chosen. Following this idea, we can divide the spectrum of an infinity system and focus on the finite system $\Sigma'(T)$ which contains the principal eigenvalue,and we have the following proposition to analyze the continuity of a finite system of eigenvalues.

Proposition A.5. *The change of a finite system $\Sigma'(T)$ of eigenvalues of a closed operator T is small (in the sense of Proposition A.1) when T is subjected to a small perturbation in the sense of generalized convergence.*

Appendix B. Proof of Lemma 3.2.

In the convergence analysis in [15], the author assumed that the deterministic $\boldsymbol{b}_0(\boldsymbol{x})$ and $c_0(\boldsymbol{x})$ satisfy $||\boldsymbol{b}_0(\boldsymbol{x})||_{L^2} \le M_1$, $|c_0(\boldsymbol{x})| \le M_2$, $||\nabla_{\boldsymbol{x}} c_0(\boldsymbol{x})||_{L^2} \le M_3$, and $||\Delta_{\boldsymbol{x}} c_0(\boldsymbol{x})||_{L^2} \le M_4$. Now we analyze these assumptions with the addition of random velocity field $\boldsymbol{v}$, and we use $\tilde{\boldsymbol{v}}$ as an approximation to $\boldsymbol{v}$ in the practical experiments.

Proof. By the triangle inequality, we can get that

$$\begin{aligned} ||\boldsymbol{b}(\boldsymbol{x},\omega)||_{L^2} &\le ||\boldsymbol{b}_0(\boldsymbol{x})||_{L^2} + ||\boldsymbol{b}(\boldsymbol{x},\omega) - \boldsymbol{b}_0(\boldsymbol{x})||_{L^2} \\ &\le M_1 + ||\boldsymbol{b}(\boldsymbol{x},\omega) - \boldsymbol{b}_0(\boldsymbol{x})||_{L^2}. \end{aligned} \tag{B.1}$$

We give the analysis for 2D cases as an example; a similar analysis can be done for higher dimensions. We assume that the deterministic part of $\boldsymbol{v}$ with period 1 is denoted as $\boldsymbol{v}_0(\boldsymbol{x})$. Thus, both $\boldsymbol{v}$ and $\tilde{\boldsymbol{v}}$ have a period $1/\Delta k \in \mathbb{N}^+$ in each spatial dimension. We define $\mathcal{D} = [0, \frac{1}{\Delta k}]^2$ and assume that both $\boldsymbol{v}$ and $\tilde{\boldsymbol{v}}$ are locally bounded in the bounded domain $\mathcal{D}$. Next, for the term $||\boldsymbol{b}(\boldsymbol{x},\omega) - \boldsymbol{b}_0(\boldsymbol{x})||_{L^2}$, we can obtain

$$\mathbb{E}_\omega[||\boldsymbol{b}(\boldsymbol{x},\omega) - \boldsymbol{b}_0(\boldsymbol{x})||_{L^2}^2] = \mathbb{E}_\omega\left[\int_{\mathcal{D}} |\boldsymbol{v}(\boldsymbol{x},\omega) - \boldsymbol{v}_0(\boldsymbol{x})|^2 d\boldsymbol{x}\right]. \tag{B.2}$$

We denote $\widehat{\boldsymbol{v}}(\boldsymbol{k},\omega) \overset{\text{def}}{=} \mathcal{F}[\boldsymbol{v}](\boldsymbol{k}), \widehat{\boldsymbol{v}}_0(\boldsymbol{k}) \overset{\text{def}}{=} \mathcal{F}[\boldsymbol{v}_0](\boldsymbol{k})$, the Fourier transform of $\boldsymbol{v}(\boldsymbol{x},\omega)$ and $\boldsymbol{v}_0(\boldsymbol{x})$. From the definition of energy spectral density, we know that $E(\boldsymbol{k}) = \mathbb{E}_\omega[|\widehat{\boldsymbol{v}}(\boldsymbol{k},\omega) - \widehat{\boldsymbol{v}}_0(\boldsymbol{k})|^2]$. Because all the spectra we consider are isotropic and have finite moments, by applying the Plancherel theorem, we can get the relationship

$$\mathbb{E}_\omega[||\boldsymbol{b}(\boldsymbol{x},\omega) - \boldsymbol{b}_0(\boldsymbol{x})||_{L^2}^2] \le 2\pi \sum_{j=0}^{+\infty} k_j E(k_j) \Delta k \le m_1, \tag{B.3}$$

where m_1 is a finite number due to $E(k)$ decaying exponentially as $k \to \infty$. Together with (B.2) and (B.3), this gives $\mathbb{E}_\omega[||\boldsymbol{b}(\boldsymbol{x},\omega)||_{L^2}] \le M_1 + \sqrt{m_1}$. The variance satisfies $Var(||\boldsymbol{b}(\boldsymbol{x},\omega)||_{L^2}) \le \mathbb{E}_\omega[||\boldsymbol{b}(\boldsymbol{x},\omega) - \boldsymbol{b}_0(\boldsymbol{x})||_{L^2}^2] \le m_1$. Then by applying Chebyshev's inequality, for a probability p

Copyright © by SIAM and ASA. Unauthorized reproduction of this article is prohibited.

Downloaded 05/24/25 to 128.195.71.97 . Redistribution subject to SIAM license or copyright; see https://epubs.siam.org/terms-privacy

close to 1, we can find the corresponding upper bound $\tilde{M}_1$, so that $P(||\boldsymbol{b}(\boldsymbol{x},\omega)||_{L^2} < \tilde{M}_1) > p$. Similar analysis can be done for $||\tilde{\boldsymbol{b}}(\boldsymbol{x},\omega)||_{L^2} = || - 2\kappa\lambda\boldsymbol{e} + \tilde{\boldsymbol{v}}||_{L^2}$, and we can get an upper bound $\tilde{M}_1'$. Then we take $M_1^* = \max(\tilde{M}_1, \tilde{M}_1')$. Thus for the second assumption, we have

$$|c(\boldsymbol{x},\omega)| \le |c_0(\boldsymbol{x})| + \lambda \cdot ||\boldsymbol{v}(\boldsymbol{x},\omega) - \boldsymbol{v}_0(\boldsymbol{x})||_{L^2} \le M_2 + \lambda \cdot ||\boldsymbol{v}(\boldsymbol{x},\omega) - \boldsymbol{v}_0(\boldsymbol{x})||_{L^2}. \tag{B.4}$$

Hence we can get $\mathbb{E}_\omega[|c(\boldsymbol{x},\omega)|] \le M_2 + \sqrt{m_1}$. The variance $Var(|c(\boldsymbol{x},\omega)|) \le \mathbb{E}_\omega[||\boldsymbol{v}(\boldsymbol{x},\omega) - \boldsymbol{v}_0(\boldsymbol{x})||_{L^2}^2] \le m_1$. By applying Chebyshev's inequality, for a probability p close to 1, we can find the corresponding upper bound $\tilde{M}_2$, so that $P(|c(\boldsymbol{x},\omega)| < \tilde{M}_2) > p$. Similar analysis can be done for $|\tilde{c}(\boldsymbol{x},\omega)|$, and we can get an upper bound $\tilde{M}_2'$. Thus we take $M_2^* = \max(\tilde{M}_2, \tilde{M}_2')$. Then for the third and fourth assumptions, we have

$$\begin{aligned} ||\nabla_{\boldsymbol{x}} c(\boldsymbol{x},\omega)||_{L^2} &\le ||\nabla_{\boldsymbol{x}} c_0(\boldsymbol{x})||_{L^2} + \lambda \cdot ||\nabla_{\boldsymbol{x}}(\boldsymbol{v}(\boldsymbol{x},\omega) - \boldsymbol{v}_0(\boldsymbol{x}))||_{L^2} \\ &\le M_3 + \lambda \cdot ||\nabla_{\boldsymbol{x}}(\boldsymbol{v}(\boldsymbol{x},\omega) - \boldsymbol{v}_0(\boldsymbol{x}))||_{L^2}, \end{aligned} \tag{B.5}$$

$$\begin{aligned} ||\Delta_{\boldsymbol{x}} c(\boldsymbol{x},\omega)||_{L^2} &\le ||\Delta_{\boldsymbol{x}} c_0(\boldsymbol{x})||_{L^2} + \lambda \cdot ||\Delta_{\boldsymbol{x}}(\boldsymbol{v}(\boldsymbol{x},\omega) - \boldsymbol{v}_0(\boldsymbol{x}))||_{L^2} \\ &\le M_4 + \lambda \cdot ||\Delta_{\boldsymbol{x}}(\boldsymbol{v}(\boldsymbol{x},\omega) - \boldsymbol{v}_0(\boldsymbol{x}))||_{L^2}. \end{aligned} \tag{B.6}$$

Hence for the terms $||\nabla_{\boldsymbol{x}}(\boldsymbol{v}(\boldsymbol{x},\omega) - \boldsymbol{v}_0(\boldsymbol{x}))||_{L^2}$ and $||\Delta_{\boldsymbol{x}}(\boldsymbol{v}(\boldsymbol{x},\omega) - \boldsymbol{v}_0(\boldsymbol{x}))||_{L^2}$, we have

$$||\nabla_{\boldsymbol{x}}(\boldsymbol{v}(\boldsymbol{x},\omega) - \boldsymbol{v}_0(\boldsymbol{x}))||_{L^2}^2 = \int_{\mathcal{D}} |\nabla_{\boldsymbol{x}}(\boldsymbol{v}(\boldsymbol{x},\omega) - \boldsymbol{v}_0(\boldsymbol{x}))|^2 d\boldsymbol{x}, \tag{B.7}$$

$$||\Delta_{\boldsymbol{x}}(\boldsymbol{v}(\boldsymbol{x},\omega) - \boldsymbol{v}_0(\boldsymbol{x}))||_{L^2}^2 = \int_{\mathcal{D}} |\Delta_{\boldsymbol{x}}(\boldsymbol{v}(\boldsymbol{x},\omega) - \boldsymbol{v}_0(\boldsymbol{x}))|^2 d\boldsymbol{x}. \tag{B.8}$$

By the properties of the Fourier transform and the Plancherel theorem, we can obtain that

$$\mathbb{E}_\omega[||\nabla_{\boldsymbol{x}}(\boldsymbol{v}(\boldsymbol{x},\omega) - \boldsymbol{v}_0(\boldsymbol{x}))||_{L^2}^2] \le 2\pi \sum_{j=0}^{\infty} k_j^3 E(k_j)\Delta k < \infty, \tag{B.9}$$

$$\mathbb{E}_\omega[||\Delta_{\boldsymbol{x}}(\boldsymbol{v}(\boldsymbol{x},\omega) - \boldsymbol{v}_0(\boldsymbol{x}))||_{L^2}^2] \le 2\pi \sum_{j=0}^{\infty} k_j^5 E(k_j)\Delta k < \infty. \tag{B.10}$$

Then we can obtain that

$$\mathbb{E}_\omega[||\nabla_{\boldsymbol{x}} c(\boldsymbol{x},\omega)||_{L^2}] \le M_3 + 2\pi \sum_{j=0}^{\infty} k_j^3 E(k_j)\Delta k, \tag{B.11}$$

$$\mathbb{E}_\omega[||\Delta_{\boldsymbol{x}} c(\boldsymbol{x},\omega)||_{L^2}] \le M_4 + 2\pi \sum_{j=0}^{\infty} k_j^5 E(k_j)\Delta k. \tag{B.12}$$

We also know the upper bound of their variance. Following the same idea, we can get $\tilde{M}_3$ and $\tilde{M}_4$; the upper bound holds with probability greater than p. Following the same idea, we can get $\tilde{M}_3'$ and $\tilde{M}_4'$. Then we take $M_3^* = \max(\tilde{M}_3, \tilde{M}_3')$ and $M_4^* = \max(\tilde{M}_4, \tilde{M}_4')$. We have already computed the assumptions' upper bound distributions after adding a random perturbation with specific energy spectral density. ∎

Copyright © by SIAM and ASA. Unauthorized reproduction of this article is prohibited.

Appendix C. Proof of Theorem 3.6.

Proof. By the operators defined in Lemma 3.3, we can get that

$$\mathcal{U}(T,0)-\prod_{h=1}^{H}e^{\Delta t_h\tilde{\mathcal{L}}(\boldsymbol{x},\omega)}e^{\Delta t_h\tilde{\mathcal{C}}(\boldsymbol{x},\omega)}=e^{\gamma T}\left(\mathcal{U}_\gamma(T,0)-\prod_{h=1}^{H}e^{\Delta t_h\tilde{\mathcal{L}}_\gamma}e^{\Delta t_h\tilde{\mathcal{C}}_\gamma}\right). \tag{C.1}$$

By the telescopic sum argument, we obtain that for any $q\in\mathcal{D}$,

$$\begin{aligned}
e_3&=\left\|\prod_{h=1}^{H}e^{\Delta t_h\mathcal{L}(\boldsymbol{x},\omega)}e^{\Delta t_h\mathcal{C}(\boldsymbol{x},\omega)}q-\prod_{h=1}^{H}e^{\Delta t_h\tilde{\mathcal{L}}(\boldsymbol{x},\omega)}e^{\Delta t_h\tilde{\mathcal{C}}(\boldsymbol{x},\omega)}q\right\|_{L^2}\\
&=e^{\gamma T}\left\|\sum_{j=1}^{H}\prod_{h=j+1}^{H}e^{\Delta t_h\mathcal{L}_\gamma}e^{\Delta t_h\mathcal{C}_\gamma}(e^{\Delta t_j\mathcal{L}_\gamma}e^{\Delta t_j\mathcal{C}_\gamma}-e^{\Delta t_j\tilde{\mathcal{L}}_\gamma}e^{\Delta t_j\tilde{\mathcal{C}}_\gamma})\prod_{i=1}^{j-1}e^{\Delta t_i\tilde{\mathcal{L}}_\gamma}e^{\Delta t_i\tilde{\mathcal{C}}_\gamma}q\right\|_{L^2}\\
&\le e^{\gamma T}\left\|\sum_{j=1}^{H}(e^{\Delta t_j\mathcal{L}_\gamma}e^{\Delta t_j\mathcal{C}_\gamma}-e^{\Delta t_j\tilde{\mathcal{L}}_\gamma}e^{\Delta t_j\tilde{\mathcal{C}}_\gamma})q\right\|_{L^2}.
\end{aligned} \tag{C.2}$$

To simplify, we denote $\mathcal{L}_\gamma=\mathcal{L}_\gamma(\boldsymbol{x},\omega)=\mathcal{L}(\boldsymbol{x},\omega)-\tilde{\gamma}$ and $\mathcal{C}_\gamma=\mathcal{C}_\gamma(\boldsymbol{x},\omega)=\mathcal{C}(\boldsymbol{x},\omega)-M_2^*$. This step is to guarantee that $||e^{\Delta t\mathcal{L}_\gamma(\boldsymbol{x},\omega)}||_{L^2}\le 1$ and $||e^{\Delta t\mathcal{C}_\gamma(\boldsymbol{x},\omega)}||_{L^2}\le 1$ are both satisfied with probability greater than p. The same holds for $\tilde{\mathcal{L}}_\gamma$ and $\tilde{\mathcal{C}}_\gamma$. By expressing the terms $e^{\Delta t\mathcal{C}_\gamma}$ and $e^{\Delta t\tilde{\mathcal{C}}_\gamma}$ in exponential series, we can obtain

$$e^{\Delta t\mathcal{L}_\gamma}e^{\Delta t\mathcal{C}_\gamma}q=e^{\Delta t\mathcal{L}_\gamma}q+(\Delta t)e^{\Delta t\mathcal{L}_\gamma}\mathcal{C}_\gamma q+r_1(\boldsymbol{x},\omega)q, \tag{C.3}$$

$$e^{\Delta t\tilde{\mathcal{L}}_\gamma}e^{\Delta t\tilde{\mathcal{C}}_\gamma}q=e^{\Delta t\tilde{\mathcal{L}}_\gamma}q+(\Delta t)e^{\Delta t\tilde{\mathcal{L}}_\gamma}\tilde{\mathcal{C}}_\gamma q+r_1'(\boldsymbol{x},\omega)q. \tag{C.4}$$

Here the residual terms are $||r_1(\boldsymbol{x},\omega)||_{L^2}\le\frac{1}{2}(\Delta t)^2||\mathcal{C}_\gamma(\boldsymbol{x},\omega)||_{L^2}^2, ||r_1'(\boldsymbol{x},\omega)||_{L^2}\le\frac{1}{2}(\Delta t)^2$ $||\tilde{\mathcal{C}}_\gamma(\boldsymbol{x},\omega)||_{L^2}^2$. Then we denote $r_1=r_1(\boldsymbol{x},\omega)$, $r_1'=r_1'(\boldsymbol{x},\omega)$ and let the two equations above subtract:

$$\begin{aligned}
LHS&=(e^{\Delta t\mathcal{L}_\gamma}-e^{\Delta t\tilde{\mathcal{L}}_\gamma})q+(\Delta t)e^{\Delta t\mathcal{L}_\gamma}\mathcal{C}_\gamma q-(\Delta t)e^{\Delta t\tilde{\mathcal{L}}_\gamma}\tilde{\mathcal{C}}_\gamma q+r_1q-r_1'q\\
&=(e^{\Delta t\mathcal{L}_\gamma}-e^{\Delta t\tilde{\mathcal{L}}_\gamma})(1+\Delta t\mathcal{C}_\gamma)q+(\Delta t)e^{\Delta t\tilde{\mathcal{L}}_\gamma}(\mathcal{C}_\gamma-\tilde{\mathcal{C}}_\gamma)q+(r_1-r_1')q.
\end{aligned} \tag{C.5}$$

Next, we define $\mathcal{G}(\boldsymbol{x},\omega)=\mathcal{L}_\gamma(\boldsymbol{x},\omega)-\tilde{\mathcal{L}}_\gamma(\boldsymbol{x},\omega)$ and $\mathcal{H}(\boldsymbol{x},\omega)=\mathcal{C}_\gamma(\boldsymbol{x},\omega)-\tilde{\mathcal{C}}_\gamma(\boldsymbol{x},\omega)$. By the freezing coefficient formula, we obtain

$$\begin{aligned}
e^{\Delta t\mathcal{L}_\gamma(\boldsymbol{x},\omega)}-e^{\Delta t\tilde{\mathcal{L}}_\gamma(\boldsymbol{x},\omega)}&=e^{\Delta t\tilde{\mathcal{L}}_\gamma(\boldsymbol{x},\omega)}+\int_0^{\Delta t}e^{s\tilde{\mathcal{L}}_\gamma(\boldsymbol{x},\omega)}\mathcal{G}(\boldsymbol{x},\omega)e^{(\Delta t-s)\mathcal{L}_\gamma(\boldsymbol{x},\omega)}ds\\
-e^{\Delta t\tilde{\mathcal{L}}_\gamma(\boldsymbol{x},\omega)}&=\int_0^{\Delta t}e^{s\tilde{\mathcal{L}}_\gamma(\boldsymbol{x},\omega)}\mathcal{G}(\boldsymbol{x},\omega)e^{(\Delta t-s)\mathcal{L}_\gamma(\boldsymbol{x},\omega)}ds.
\end{aligned} \tag{C.6}$$

We denote $\mathcal{G}=\mathcal{G}(\boldsymbol{x},\omega)$, $\mathcal{H}=\mathcal{H}(\boldsymbol{x},\omega)$. Then we substitute the above equation (C.6) into (C.5) and compute its L^2 norm.

Downloaded 05/24/25 to 128.195.71.97 . Redistribution subject to SIAM license or copyright; see https://epubs.siam.org/terms-privacy

Copyright © by SIAM and ASA. Unauthorized reproduction of this article is prohibited.

$$
\begin{aligned}
&||(e^{\Delta t\mathcal{L}_\gamma}-e^{\Delta t\tilde{\mathcal{L}}_\gamma})(1+\Delta t\mathcal{C}_\gamma)q+(\Delta t)e^{\Delta t\tilde{\mathcal{L}}_\gamma}(\mathcal{C}_\gamma-\tilde{\mathcal{C}}_\gamma)q+(r_1-r_1')q||_{L^2}\\
&\quad\le||(e^{\Delta t\mathcal{L}_\gamma}-e^{\Delta t\tilde{\mathcal{L}}_\gamma})(1+\Delta t\mathcal{C}_\gamma)q||_{L^2}+||(\Delta t)e^{\Delta t\tilde{\mathcal{L}}_\gamma}\mathcal{H}q||_{L^2}+||(r_1-r_1')q||_{L^2}\\
&\quad\le||(e^{\Delta t\mathcal{L}_\gamma}-e^{\Delta t\tilde{\mathcal{L}}_\gamma})(1+\Delta t\mathcal{C}_\gamma)q||_{L^2}+(\Delta t)||\mathcal{H}q||_{L^2}\\
&\qquad+\frac{1}{2}(\Delta t)^2(||\mathcal{C}_\gamma||_{L^2}^2+||\tilde{\mathcal{C}}_\gamma||_{L^2}^2)||q||_{L^2}\\
&\quad\le(\Delta t)||\mathcal{G}q||_{L^2}+(\Delta t)^2||\mathcal{G}\mathcal{C}_\gamma q||_{L^2}+(\Delta t)||\mathcal{H}q||_{L^2}\\
&\qquad+\frac{1}{2}(\Delta t)^2(||\mathcal{C}_\gamma||_{L^2}^2+||\tilde{\mathcal{C}}_\gamma||_{L^2}^2)||q||_{L^2}.
\end{aligned}
\tag{C.7}
$$

Then we substitute this result back into (C.2), and we can get the error estimate

$$
\begin{aligned}
e_3&=\left|\left|\prod_{h=1}^{H}e^{\Delta t_h\mathcal{L}(\boldsymbol{x},\omega)}e^{\Delta t_h\mathcal{C}(\boldsymbol{x},\omega)}q-\prod_{h=1}^{H}e^{\Delta t_h\tilde{\mathcal{L}}(\boldsymbol{x},\omega)}e^{\Delta t_h\tilde{\mathcal{C}}(\boldsymbol{x},\omega)}q\right|\right|_{L^2}\\
&\le C_1(q,\omega)\Delta t+C_2(||\mathcal{G}q||_{L^2}+||\mathcal{H}q||_{L^2}).
\end{aligned}
\tag{C.8}
$$

Here the coefficients are $C_1(q,\omega)=Te^{\gamma T}\cdot(||\mathcal{G}(\boldsymbol{x},\omega)\mathcal{C}_\gamma(\boldsymbol{x},\omega)q||_{L^2}+\frac{1}{2}(||\mathcal{C}_\gamma(\boldsymbol{x},\omega)||_{L^2}^2+||\tilde{\mathcal{C}}_\gamma(\boldsymbol{x},\omega)||_{L^2}^2)||q||_{L^2})$, $C_2=Te^{\gamma T}$. Then due to the fact that $||\tilde{\mathcal{C}}_\gamma(\boldsymbol{x},\omega)||_{L^2}^2$, $||\mathcal{C}_\gamma(\boldsymbol{x},\omega)||_{L^2}^2<1$ are both satisfied with probability greater than p, we can obtain that $prob(B_1)>p$, where

$$
B_1=\left\{e_3\le Te^{\gamma T}\cdot(||\boldsymbol{v}-\tilde{\boldsymbol{v}}||_{L^2}\cdot(||\nabla_{\boldsymbol{x}}q||_{L^2}+\lambda||q||_{L^2})+(\Delta t)(||\boldsymbol{v}-\tilde{\boldsymbol{v}}||_{L^2}\cdot||\nabla_{\boldsymbol{x}}q||_{L^2}+||q||_{L^2}))\right\}.
\tag{C.9}
$$

■

Appendix D. Proof of Theorem 3.8.

Proof.

$$
\begin{aligned}
&e^{\Delta t\mathcal{L}_\gamma^j}e^{\Delta t\mathcal{C}_\gamma^j}-e^{\Delta t\mathcal{L}_\gamma}e^{\Delta t\mathcal{C}_\gamma}=e^{\Delta t\mathcal{L}_\gamma}e^{\Delta t\mathcal{C}_\gamma}[e^{-\Delta t\mathcal{C}_\gamma}e^{-\Delta t\mathcal{L}_\gamma}-e^{-\Delta t\mathcal{C}_\gamma^j}e^{-\Delta t\mathcal{L}_\gamma^j}]e^{\Delta t\mathcal{L}_\gamma^j}e^{\Delta t\mathcal{C}_\gamma^j}\\
&\quad=e^{\Delta t\mathcal{L}_\gamma}e^{\Delta t\mathcal{C}_\gamma}[e^{-\Delta t\mathcal{C}_\gamma}e^{-\Delta t\mathcal{L}_\gamma}-e^{-\Delta t\mathcal{C}_\gamma^j}e^{-\Delta t\mathcal{L}_\gamma^j}]e^{\Delta t\mathcal{L}_\gamma}e^{\Delta t\mathcal{C}_\gamma}\\
&\qquad+e^{\Delta t\mathcal{L}_\gamma}e^{\Delta t\mathcal{C}_\gamma}[e^{-\Delta t\mathcal{C}_\gamma}e^{-\Delta t\mathcal{L}_\gamma}-e^{-\Delta t\mathcal{C}_\gamma^j}e^{-\Delta t\mathcal{L}_\gamma^j}][e^{\Delta t\mathcal{L}_\gamma^j}e^{\Delta t\mathcal{C}_\gamma^j}-e^{\Delta t\mathcal{L}_\gamma}e^{\Delta t\mathcal{C}_\gamma}].
\end{aligned}
\tag{D.1}
$$

Now applying $e^{\Delta t\mathcal{L}_\gamma^j}e^{\Delta t\mathcal{C}_\gamma^j}-e^{\Delta t\mathcal{L}_\gamma}e^{\Delta t\mathcal{C}_\gamma}$ on q, we can get

$$
\begin{aligned}
||e^{\Delta t\mathcal{L}_\gamma^j}e^{\Delta t\mathcal{C}_\gamma^j}q-e^{\Delta t\mathcal{L}_\gamma}e^{\Delta t\mathcal{C}_\gamma}q||_{L^2}&\le||e^{-\Delta t\mathcal{C}_\gamma}e^{-\Delta t\mathcal{L}_\gamma}-e^{-\Delta t\mathcal{C}_\gamma^j}e^{-\Delta t\mathcal{L}_\gamma^j}||_{L^2}\\
&\cdot||e^{\Delta t\mathcal{L}_\gamma}e^{\Delta t\mathcal{C}_\gamma}||_{L^2}^2\cdot||q||_{L^2}+||e^{\Delta t\mathcal{L}_\gamma}e^{\Delta t\mathcal{C}_\gamma}||_{L^2}\\
&\cdot||e^{-\Delta t\mathcal{C}_\gamma}e^{-\Delta t\mathcal{L}_\gamma}-e^{-\Delta t\mathcal{C}_\gamma^j}e^{-\Delta t\mathcal{L}_\gamma^j}||_{L^2}\cdot||e^{\Delta t\mathcal{L}_\gamma^j}e^{\Delta t\mathcal{C}_\gamma^j}q-e^{\Delta t\mathcal{L}_\gamma}e^{\Delta t\mathcal{C}_\gamma}q||_{L^2}.
\end{aligned}
\tag{D.2}
$$

Then for the term $||e^{-\Delta t\mathcal{C}_\gamma}e^{-\Delta t\mathcal{L}_\gamma}-e^{-\Delta t\mathcal{C}_\gamma^j}e^{-\Delta t\mathcal{L}_\gamma^j}||_{L^2}$, we can define $C_\gamma=e^{2\gamma\Delta t}$,$\mathcal{C}_{\bar{\gamma}}=\mathcal{C}+M_2^*$, $\mathcal{L}_{\bar{\gamma}}=\mathcal{L}+\tilde{\gamma}$ and similarly get $\mathcal{C}_{\bar{\gamma}}^j$ and $\mathcal{L}_{\bar{\gamma}}^j$. Here M_2^* and $\tilde{\gamma}$ are the upper bound defined in Lemma 3.3. Thus following the idea above, we can get

$$
||e^{-\Delta t\mathcal{C}_\gamma}e^{-\Delta t\mathcal{L}_\gamma}-e^{-\Delta t\mathcal{C}_\gamma^j}e^{-\Delta t\mathcal{L}_\gamma^j}||_{L^2}=C_\gamma||e^{-\Delta t\mathcal{C}_{\bar{\gamma}}}e^{-\Delta t\mathcal{L}_{\bar{\gamma}}}-e^{-\Delta t\mathcal{C}_{\bar{\gamma}}^j}e^{-\Delta t\mathcal{L}_{\bar{\gamma}}^j}||_{L^2}.
\tag{D.3}
$$

Next, we can estimate $||e^{-\Delta t\mathcal{C}_{\bar{\gamma}}}e^{-\Delta t\mathcal{L}_{\bar{\gamma}}}-e^{-\Delta t\mathcal{C}_{\bar{\gamma}}^j}e^{-\Delta t\mathcal{L}_{\bar{\gamma}}^j}||_{L^2}$ following the idea mentioned in (C.3)–(C.7). Here we need to emphasize that for higher-order terms of Δt in the expansion,

Downloaded 05/24/25 to 128.195.71.97 . Redistribution subject to SIAM license or copyright; see https://epubs.siam.org/terms-privacy

Copyright © by SIAM and ASA. Unauthorized reproduction of this article is prohibited.

we still end up with the factor $||\boldsymbol{v}-\boldsymbol{v}_j||_{L^2}$. So, we can get that $\lim_{j\to\infty}||e^{-\Delta t\mathcal{C}_{\bar{\gamma}}}e^{-\Delta t\mathcal{L}_{\bar{\gamma}}}-e^{-\Delta t\mathcal{C}^j_{\bar{\gamma}}}e^{-\Delta t\mathcal{L}^j_{\bar{\gamma}}}||_{L^2}=0$. Then we can assume, for $j\geq N^*$,

$$||e^{\Delta t\mathcal{L}_\gamma}e^{\Delta t\mathcal{C}_\gamma}||_{L^2}\cdot||e^{-\Delta t\mathcal{C}_\gamma}e^{-\Delta t\mathcal{L}_\gamma}-e^{-\Delta t\mathcal{C}^j_\gamma}e^{-\Delta t\mathcal{L}^j_\gamma}||_{L^2}\leq\frac{1}{2}. \tag{D.4}$$

Then by substituting back into (D.2), we can get, $\forall j\geq N^*$,

$$\begin{aligned}||e^{\Delta t\mathcal{L}^j_\gamma}e^{\Delta t\mathcal{C}^j_\gamma}q-e^{\Delta t\mathcal{L}_\gamma}e^{\Delta t\mathcal{C}_\gamma}q||_{L^2}\leq 2\,&||e^{-\Delta t\mathcal{C}_\gamma}e^{-\Delta t\mathcal{L}_\gamma}-e^{-\Delta t\mathcal{C}^j_\gamma}e^{-\Delta t\mathcal{L}^j_\gamma}||_{L^2}\\ &\cdot||e^{\Delta t\mathcal{L}_\gamma}e^{\Delta t\mathcal{C}_\gamma}||^2_{L^2}\cdot||q||_{L^2}.\end{aligned} \tag{D.5}$$

Hence we can get, $\forall j\geq N^*$,

$$||e^{\Delta t\mathcal{L}^j_\gamma}e^{\Delta t\mathcal{C}^j_\gamma}q-e^{\Delta t\mathcal{L}_\gamma}e^{\Delta t\mathcal{C}_\gamma}q||_{L^2}\leq 2||e^{-\Delta t\mathcal{C}_\gamma}e^{-\Delta t\mathcal{L}_\gamma}-e^{-\Delta t\mathcal{C}^j_\gamma}e^{-\Delta t\mathcal{L}^j_\gamma}||_{L^2}\cdot||q||_{L^2}, \tag{D.6}$$

so that for $||e^{\Delta t\mathcal{L}^j_\gamma}e^{\Delta t\mathcal{C}^j_\gamma}q-e^{\Delta t\mathcal{L}_\gamma}e^{\Delta t\mathcal{C}_\gamma}q||_{L^2}$, it will have a convergence rate $O(||\boldsymbol{v}-\boldsymbol{v}_j||\cdot(\Delta t+(\Delta t)^2))$. Then for $2||e^{-\Delta t\mathcal{C}_\gamma}e^{-\Delta t\mathcal{L}_\gamma}-e^{-\Delta t\mathcal{C}^j_\gamma}e^{-\Delta t\mathcal{L}^j_\gamma}||_{L^2}\cdot||q||_{L^2}$, we have

$$\begin{aligned}LHS&=2e^{2\gamma\Delta t}||e^{-\Delta t\mathcal{C}_{\bar{\gamma}}}e^{-\Delta t\mathcal{L}_{\bar{\gamma}}}-e^{-\Delta t\mathcal{C}^j_{\bar{\gamma}}}e^{-\Delta t\mathcal{L}^j_{\bar{\gamma}}}||_{L^2}\cdot||q||_{L^2}\\ &\leq 2e^{2\gamma\Delta t}\Big[\Delta t||\mathcal{G}||_{L^2}+(\Delta t)^2||\mathcal{C}_{\bar{\gamma}}\mathcal{G}||_{L^2}+\Delta t||\mathcal{H}||_{L^2}\\ &\quad+\frac{1}{2}(\Delta t)^2(||\mathcal{C}_{\bar{\gamma}}||_{L^2}+||\mathcal{C}^j_{\bar{\gamma}}||_{L^2})\Big]\cdot||q||_{L^2}.\end{aligned} \tag{D.7}$$

Here $\mathcal{G}$ and $\mathcal{H}$ are defined as in (3.30). Then for the entire evolution process, we can obtain that

$$\begin{aligned}e_3&\leq 2Te^{\gamma(T+2\Delta t)}\Big[||\mathcal{G}||_{L^2}+(\Delta t)||\mathcal{C}_{\bar{\gamma}}\mathcal{G}||_{L^2}+||\mathcal{H}||_{L^2}\\ &\quad+\frac{\Delta t}{2}(||\mathcal{C}_{\bar{\gamma}}||_{L^2}+||\mathcal{C}^j_{\bar{\gamma}}||_{L^2})\Big]\cdot||q||_{L^2}\\ &\leq 2Te^{\gamma(T+2\Delta t)}[2M_2^*\Delta t+||\boldsymbol{v}-\boldsymbol{v}_j||_{L^2}(C_D(p)+\lambda)\\ &\quad+2M_2^*C_D(p)\Delta t||\boldsymbol{v}-\boldsymbol{v}_j||_{L^2}]\cdot||q||_{L^2}.\end{aligned} \tag{D.8}$$

Here $C_D(p)$ is a constant that depends on the selection of γ, which means it will depend on p. Then we can get

$$\begin{aligned}e_3&\leq 2Te^{\gamma(T+2\Delta t)}[(M_2^*)^2(\Delta t)^2+2M_2^*\Delta t+(C_D(p)+\lambda)||\boldsymbol{v}-\boldsymbol{v}_j||_{L^2}\\ &\quad+C_D(p)^2||\boldsymbol{v}-\boldsymbol{v}_j||^2_{L^2}]\cdot||q||_{L^2}.\end{aligned} \tag{D.9}$$

Since $\lim_{\Delta t\to 0}\frac{(M_2^*)^2(\Delta t)^2}{2M_2^*\Delta t}=0$ and $\lim_{j\to\infty}\frac{C_D(p)^2||\boldsymbol{v}-\boldsymbol{v}_j||^2_{L^2}}{(C_D(p)+\lambda)||\boldsymbol{v}-\boldsymbol{v}_j||_{L^2}}=0$, as $\Delta t\to 0$ and $j\to\infty$, we have

$$e_3\leq 2Te^{\gamma(T+2\Delta t)}[2M_2^*\Delta t+(C_D(p)+\lambda)||\boldsymbol{v}-\boldsymbol{v}_j||_{L^2}]\cdot||q||_{L^2}+O((\Delta t)^2)+O(||\boldsymbol{v}-\boldsymbol{v}_j||^2_{L^2}). \tag{D.10}$$

Downloaded 05/24/25 to 128.195.71.97 . Redistribution subject to SIAM license or copyright; see https://epubs.siam.org/terms-privacy

Copyright © by SIAM and ASA. Unauthorized reproduction of this article is prohibited.

By applying the Cauchy–Schwarz inequality, we can get

$$2M_2^*\Delta t + (C_D(p)+\lambda)||\boldsymbol{v}-\boldsymbol{v}_j||_{L^2} \le \sqrt{4(M_2^*)^2+(C_D(p)+\lambda)^2}\sqrt{(\Delta t)^2+||\boldsymbol{v}-\boldsymbol{v}_j||_{L^2}^2}. \tag{D.11}$$

By denoting $C_3(\lambda,p) = 4Te^{\gamma(T+1)}\cdot\sqrt{4(M_2^*)^2+(C_D(p)+\lambda)^2}$, we can obtain (3.40). Then due to the error estimate of e_1, e_2, and $O(\frac{4C_s}{3}(\Delta t)^{\frac{1}{2}}+2M_2^*\Delta t) = O(\frac{4C_s}{3}(\Delta t)^{\frac{1}{2}})$, the total error estimate e_{op} in approximating the solution operator $\mathcal{U}(T,0)$ will be

$$e_{op} = O\left(\frac{4C_s}{3}(\Delta t)^{\frac{1}{2}}\right) + O((C_D(p)+\lambda)||\boldsymbol{v}-\boldsymbol{v}_j||_{L^2}). \tag{D.12}$$

REFERENCES

[1] H. Berestycki, F. Hamel, and N. Nadirashvili, *The speed of propagation for KPP type problems. I: Periodic framework*, J. Eur. Math. Soc., 7 (2005), pp. 173–213, https://doi.org/10.4171/jems/26.

[2] F. Cérou, P. Del Moral, and A. Guyader, *A nonasymptotic theorem for unnormalized Feynman–Kac particle models*, Ann. Inst. H. Poincaré Probab. Statist.,47 (2011), pp. 629–649, https://doi.org/10.1214/10-AIHP358.

[3] T. Dombre, U. Frisch, J. Greene, M. Hénon, A. Mehr, and A. Soward, *Chaotic streamlines in the ABC flows*, J. Fluid Mech., 167 (1986), pp. 353–391, https://doi.org/10.1017/S0022112086002859.

[4] G. Ferré and G. Stoltz, *Error estimates on ergodic properties of discretized Feynman–Kac semigroups*, Numer. Math., 143 (2019), pp. 261–313, https://doi.org/10.1007/s00211-019-01059-1.

[5] M. Freidlin, *Functional Integration and Partial Differential Equations,* Ann. Math. Stud. 109, Princeton University Press, 1985.

[6] J. Gärtner and M. Freidlin, *On the propagation of concentration waves in periodic and random media*, Dokl. Akad. Nauk SSSR, 249 (1979), pp. 521–525 (in Russian), https://www.mathnet.ru/eng/dan/v249/i3/p521.

[7] A. Gloria and F. Otto, *Quantitative estimate on the periodic approximation of the corrector in stochastic homogenization*, ESAIM Proc Surv., 48 (2015), pp. 89–97, https://doi.org/10.1051/proc/201448003.

[8] P. Hess, *Periodic-Parabolic Boundary Value Problems and Positivity*, Pitman Res. Notes Math. Ser. 247, Longman Scientific & Technical, 1991.

[9] C. Kao, Y. Liu, and J. Xin, *A semi-Lagrangian computation of front speeds of G-equation in ABC and Kolmogorov flows with estimation via ballistic orbits*, SIAM J. Multiscale Model. Simul., 20 (2022), pp. 107–117, https://doi.org/10.1137/20M1387699.

[10] T. Kato, *Perturbation Theory for Linear Operators*, Classics Math. 132, Springer, 1995, https://doi.org/10.1007/978-3-642-66282-9.

[11] V. Khoromskaia, B. Khoromskij, and F. Otto, *Numerical study in stochastic homogenization for elliptic partial differential equations: Convergence rate in the size of representative volume elements*, Numer. Linear Algebra Appl., 27 (2020), e2296, https://doi.org/10.1002/nla.2296.

[12] A. Kolmogorov, I. Petrovsky, and N. Piskunov, *Investigation of the equation of diffusion combined with increasing of the substance and its application to a biology problem*, Bull. Moscow State Univ. Ser. A Math. Mech., 1 (1937), pp. 1–25.

[13] J. Lu, F. Otto, and L. Wang, *Optimal artificial boundary conditions based on second-order correctors for three dimensional random elliptic media*, Comm. Partial Differential Equations, 49 (2024), pp. 609–670, https://doi.org/10.1080/03605302.2024.2374568.

[14] J. Lyu, Z. Wang, J. Xin, and Z. Zhang, *Convergence analysis of stochastic structure-preserving schemes for computing effective diffusivity in random flows*, SIAM J. Numer. Anal., 58 (2020), pp. 3040–3067, https://doi.org/10.1137/19M1277163.

[15] J. Lyu, Z. Wang, J. Xin, and Z. Zhang, *A convergent interacting particle method and computation of KPP front speeds in chaotic flows*, SIAM J. Numer. Anal., 60 (2022), pp. 1136–1167, https://doi.org/10.1137/21M1410786.

Downloaded 05/24/25 to 128.195.71.97 . Redistribution subject to SIAM license or copyright; see https://epubs.siam.org/terms-privacy

Copyright © by SIAM and ASA. Unauthorized reproduction of this article is prohibited.

[16] A. Majda and P. Kramer, *Simplified models for turbulent diffusion: Theory, numerical modelling, and physical phenomena*, Phys. Rep., 314 (1999), pp. 237–574, https://doi.org/10.1016/S0370-1573(98)00083-0.
[17] A. Majda and P. Souganidis, *Large scale front dynamics for turbulent reaction-diffusion equations with separated velocity scales*, Nonlinearity, 7 (1994), pp. 1–30, https://doi.org/10.1088/0951-7715/7/1/001.
[18] T. McMillen, J. Xin, Y. Yu, and A. Zlatoš, *Ballistic orbits and front speed enhancement for ABC flows*, SIAM J. Appl. Dyn. Syst., 15 (2016), pp. 1753–1782, https://doi.org/10.1137/16M1059059.
[19] S. Meyn and R. L. Tweedie, *Stochastic Stability of Markov Chains*, Springer, 1992.
[20] G. Milstein, J. Schoenmakers, and V. Spokoiny, *Transition density estimation for stochastic differential equations via forward-reverse representations*, Bernoulli, 10 (2004), pp. 281–312, https://doi.org/10.3150/bj/1082380220.
[21] P. D. Moral and L. Miclo, *Branching and interacting particle systems approximations of Feynman-Kac formulae with applications to non-linear filtering*, in)Séminaire de Probabilités XXXIV, Lecture Notes in Math. 1729, Springer-Verlag, 2000, pp. 1–145.
[22] J. Nolen, J.-M. Roquejoffre, L. Ryzhik, and A. Zlatoš, *Existence and non-existence of Fisher-KPP transition fronts*, Arch. Ration. Mech. Anal., 203 (2012), pp. 217–246, https://doi.org/10.1007/s00205-011-0449-4.
[23] J. Nolen and J. Xin, *A variational principle for KPP front speeds in temporally random shear flows*, Comm. Math. Phys., 269 (2007), pp. 493–532, https://doi.org/10.1007/s00220-006-0144-8.
[24] J. Nolen and J. Xin, *Computing reactive front speeds in random flows by variational principle*, Phys. D, 237 (2008), pp. 3172–3177, https://doi.org/10.1016/j.physd.2008.04.024.
[25] J. Nolen and J. Xin, *Asymptotic spreading of KPP reactive fronts in incompressible space-time random flows*, Ann Inst. H. Poincaré, Anal. Non Linéaire, 26 (2009), pp. 815–839, https://doi.org/10.1016/j.anihpc.2008.02.005.
[26] A. Novikov and L. Ryzhik, *Boundary layers and KPP fronts in a cellular flow*, Arch. Ration. Mech. Anal., 184 (2007), pp. 23–48, https://doi.org/10.1007/s00205-006-0038-0.
[27] G. Pavliotis and A. Stuart, *Periodic homogenization for inertial particles*, Phys. D, 204 (2005), pp. 161–187, https://doi.org/10.1016/j.physd.2005.04.011.
[28] G. Pavliotis and A. Stuart, *Homogenization for inertial particles in a random flow*, Commun. Math. Sci., 5 (2007), pp. 507–531, https://doi.org/10.4310/CMS.2007.v5.n3.a1.
[29] G. Pavliotis, A. Stuart, and K. Zygalakis, *Calculating effective diffusivities in the limit of vanishing molecular diffusion*, J. Comput. Phys., 228 (2009), pp. 1030–1055, https://doi.org/10.1016/j.jcp.2008.10.014.
[30] L. Shen, J. Xin, and A. Zhou, *Finite element computation of KPP front speeds in 3D cellular and ABC flows*, Math. Model. Nat. Phenom., 8 (2013), pp. 182–197, https://doi.org/10.1051/mmnp/20138311.
[31] L. Shen, J. Xin, and A. Zhou, *Finite element computation of KPP front speeds in cellular and cat's eye flows*, J. Sci. Comput., 55 (2013), pp. 455–470, https://doi.org/10.1007/s10915-012-9641-4.
[32] Z. Wang, J. Xin, and Z. Zhang, *Computing effective diffusivity of chaotic and stochastic flows using structure-preserving schemes*, SIAM J. Numer. Anal., 56 (2018), pp. 2322–2344, https://doi.org/10.1137/18M1165219.
[33] Z. Wang, J. Xin, and Z. Zhang, *Sharp error estimates on a stochastic structure-preserving scheme in computing effective diffusivity of 3D chaotic flows*, Multiscale Model. Simul., 93 (2021), pp. 1167–1189, https://doi.org/10.1137/19M1275516.
[34] Z. Wang, J. Xin, and Z. Zhang, *Computing effective diffusivities in 3D time-dependent chaotic flows with a convergent Lagrangian numerical method*, ESAIM Math. Model. Numer. Anal., 56 (2022), pp. 1521–1544, https://doi.org/10.1051/m2an/2022049.
[35] J. Xin, *Existence of planar flame fronts in convective-diffusive periodic media*, Arch. Ration. Mech. Anal., 121 (1992), pp. 205–233, https://doi.org/10.1007/BF00410613.
[36] J. Xin, *Front propagation in heterogeneous media*, SIAM Rev., 42 (2000), pp. 161–230, https://doi.org/10.1137/S0036144599364296.
[37] J. Xin, *An Introduction to Fronts in Random Media*, Surv. Tutor. Appl. Math. Sci. 5 5, Springer, 2009.
[38] J. Xin, Y. Yu, and A. Zlatoš, *Periodic orbits of the ABC flow with* $A = B = C = 1$, SIAM J. Math. Anal., 48 (2016), pp. 4087–4093, https://doi.org/10.1137/16M1076241.

Downloaded 05/24/25 to 128.195.71.97 . Redistribution subject to SIAM license or copyright; see https://epubs.siam.org/terms-privacy

Copyright © by SIAM and ASA. Unauthorized reproduction of this article is prohibited.

[39] A. M. Yaglom, *Correlation Theory of Stationary and Related Random Functions. Vol.* 1 *Basic Results*, Springer Ser. Statist., Springer-Verlag, 1987.

[40] T. Zhang, Z. Wang, J. Xin, and Z. Zhang, *A Structure-Preserving Scheme for Computing Effective Diffusivity and Anomalous Diffusion Phenomena of Random Flows*, preprint, arXiv:2405.19003, 2024.

[41] P. Zu, L. Chen, and J. Xin, *A computational study of residual KPP front speeds in time-periodic cellular flows in the small diffusion limit*, Phys. D, 311-312 (2015), pp. 37–44, https://doi.org/10.1016/j.physd.2015.07.001.

Downloaded 05/24/25 to 128.195.71.97 . Redistribution subject to SIAM license or copyright; see https://epubs.siam.org/terms-privacy

Copyright © by SIAM and ASA. Unauthorized reproduction of this article is prohibited.